ABSTRACT

Demonstration of a Power Conditioning System
for Grid-connected Fuel Cell Power Plant

Guiying Wu, M.S.E.C.E.

Mentor: Kwang Y. Lee, Ph.D.

This thesis demonstrates a power conditioning system (PCS) for grid-connected hybrid direct fuel-cell with turbine (DFC/T) power plant. The PCS is an interface between distributed generation and utility grid. It regulates voltage, current and power transmitted from the hybrid DFC/T power plant to utility grid. The proposed system consists of DC/DC converters, DC/AC inverter, and an LCL filter. The DC/DC converter and DC/AC inverter use switches that operate at high speeds. The use of detailed model with switches will decrease the simulation speed, thus it takes long time to execute time simulations in MATLAB. This thesis utilizes effective averaged models for converter and inverter to reduce the calculation time for a large-scale fuel cell power plant in MATLAB. To regulate and stabilize the DC bus voltage, DC/DC converter with PI controller is adopted. For the DC/AC inverter, active and reactive power flow controller is used.

Demonstration of a Power Conditioning System
for Grid-connected Fuel Cell Power Plant

by

Guiying Wu, B.S.

A Thesis

Approved by the Department of Electrical and Computer Engineering

_____

Kwang Y. Lee, Ph.D., Chairperson

Submitted to the Graduate Faculty of
Baylor University in Partial Fulfillment of the
Requirements for the Degree
of

Master of Science in Electrical and Computer Engineering

Approved by the Thesis Committee

_____

Kwang Y. Lee, Ph.D., Chairperson

_____

Mack Grady, Ph.D.

_____

Paul C. Grabow, Ph.D.

Accepted by the Graduate School

August 2013

_____

J. Larry Lyon, Ph.D., Dean

Page bearing signatures is kept on file in the Graduate School.

TABLE OF CONTENTS

LIST OF FIGURES vi
LIST OF TABLES viii
LIST OF ABBREVIATIONS ix
LIST OF PARAMETERS xi
ACKNOWLEDGMENTS xiv
CHAPTER ONE 1
Introduction 1
1.1 Motivation 1
1.2 Background 2
1.3 Recent Researches and Achievements 7
1.4 Thesis Organization 7
CHAPTER TWO 8
Averaged Model of DC/DC Converter 8
2.1 Introduction to DC/DC Converter 8
2.2 The Averaged Model of Buck-Boost Converter 10
2.3 Converter Controller Design 14
2.4 Parameters for Buck-Boost Converter and Control System 15
CHAPTER THREE 19
Averaged Model of Three-phase Inverter 19
3. 1 Introduction to Voltage Source Inverters 19
3. 2 The Averaged Model of Three-Phase Inverter 22
3. 3 Simplified Model of Three-Phase VSI 24
CHAPTER FOUR 26
Power Flow Control of Grid-connected Fuel Cell Power Plant 26
4. 1 Introduction 26
4. 2 Power Flow Control through Current Regulation 26
4. 3 Power Flow Control through Voltage Regulation 28
4. 4 Fuel-Cell Power Plant Connected to the Grid 30
CHAPTER FIVE 33
Phase Locked Loop 33
5. 1 Introduction to Phase Locked Loop 33
5. 2 Three-Phase PLL Design 33

CHAPTER SIX 38
Simulation Results 38
6. 1 DC Bus Voltage 38
6. 2 Real and Reactive Power Flow Control 40
6. 3 Comparison with Detailed Model 47
CHAPTER SEVEN 49
Conclusion and Future Work 49
7.1 Conclusions 49
7.2 Future Work 49
APPENDIX 52
The PCS in Matlab Simulink 52
BIBLIOGRAPHY 53

LIST OF FIGURES

Figure 1: Structure of Fuel Cell Stack with Turbine Power Plant. 5

Figure 2: The overall diagram of fuel cell power plant and PCS. 6

Figure 3: The overall structure of the PCS. 7

Figure 4: PWM Signal Generator 9

Figure 5: Fuel Cell Stack Output Voltage..... 11

Figure 6: Topology of Buck-Boost DC/DC Converter. 12

Figure 7: Case for the switch-on condition. 13

Figure 8: Case for the switch-off condition. 13

Figure 9: The scheme of the converter controller. 14

Figure 10: Block diagram of the converter control. 15

Figure 11: Bode Diagram of the Control System for Buck-Boost Converter. 18

Figure 12: Three Phase Full-Bridge Inverter. 19

Figure 13: Three-Phase SPWM Wave. 21

Figure 14: Averaged equivalent circuit of an inverter arm. 22

Figure 15: Averaged equivalent circuit in the three-phase VSI. 23

Figure 16: Simplified model of the inverter. 25

Figure 17: Block Diagram of Current Control. 28

Figure 18: Power flow between two sources. 29

Figure 19: Scheme of PQ controller for inverter. 30

Figure 20: Fuel Cell Power Plant integrated into Grid. 31

Figure 21: VSI connected to Grid. 32

Figure 22: Phase Locked Loop. 34

Figure 23: Flow diagram of the basic operation of the PCS. 39

Figure 24: DC bus Voltage. 40

Figure 25: Short-time simulation for real power. 41

Figure 26: Short-time simulation for reactive power. 42

Figure 27: Long-time simulation for real power. 42

Figure 28: Long-time simulation for reactive power. 43

Figure 29: Real and Reactive Power of Load Demand. 44

Figure 30: Real and Reactive Power of PV Bus. 45

Figure 31: The Voltage Magnitude and Phase Angle of PV bus. 45

Figure 32: Simulation of real power for fuel cell considered as a generator. 46

Figure 33: Simulation of reactive power for fuel cell considered as a generator. 46

Figure 34: Comparison of the real power output of two models. 48

Figure 35: Comparison of the reactive power output of two models. 48

Figure 36: The PCS in Matlab Simulink 52

LIST OF TABLES

Table 1: Parameters of DC/DC Converter and Control System. 17

Table 2: Bus input Data. 31

Table 3: Line input Data. 31

Table 4:The Comparison of the Elapsed Time between the Detailed and Averaged Model. 47

LIST OF ABBREVIATIONS

AC - Alternating Current

AFC - Alkali Fuel Cells

CSI - Current Source Inverter

D - Duty Cycle

DC - Direct Current

DFC - Direct Fuel Cell

DFC/T - Direct Fuel Cell with Turbine

DG - Distributed Generation

ESR - Equivalent Series Resistance

IGBT - Insulated Gate Bipolar Transistor

MCFC - Molten Carbonate Fuel Cells

MOSFET - Metal Oxide Semiconductor Field Effect Transistor

PAFC - Phosphoric Acid fuel cells

PCS - Power Conditioning System

PEMFC - Proton Exchange Membrane fuel cells

PI - Proportional Integral

PLL - Phase Locked Loop

PWM - Pulse Width Modulation

SOFC - Solid Oxide fuel cells

SPWM - Sinusoidal Pulse Width Modulation

VCO - Voltage Controlled Oscillator

VSI - Voltage Source Inverter

LIST OF PARAMETERS

C - The capacitor in the DC/DC converter.

C_f - The capacitor in the LCL filter.

D - Duty ratio.

d_a, d_b, d_c - The duty cycle of the averaged equivalent circuit in the VSI.

f_s - The switching frequency for PWM or SPWM generator.

K_{qd}, K_{dq} – The decoupling terms in the current regulation.

i_{abc} - The three-phase current in transmission line.

i_c – The current in the LCL filter.

i_{dc} – The current in DC bus.

i_{dq} - The current in *dq0*-frame.

$i_{dq,\,ref}$ - The current reference in *dq0*-frame.

$i_{g,abc}$ - The three-phase current at the grid side.

$i_{i,abc}$ - The three-phase current at the inverter side.

$i_{f,abc}$ – The current in the LCL filter.

i_L - The current in the inductor.

I_o – The output current of DC/DC converter.

L - The inductor in the DC/DC converter.

L_i - The inductor at the inverter side in the LCL filter.

L_g - The inductor at the grid side in the LCL filter.

L_l - The reactance of the LCL filter, transformer and transmission line.

R_{eq} - The equivalent load of the DC/DC converter.

R_f – The resistance in the LCL filter.

R_g - The ESR of the inductor at the grid side.

R_i - The ESR of the inductor at the inverter side.

R_L - The ESR of the inductor.

T_s - Time period for one switching cycle.

$T_1, T_2, T_3, T_4, T_5, T_6$ - The switching devices in the three-phase inverter.

v_c - Voltage of the capacitor.

V_{dc} - DC link voltage.

V_{fc} - The output voltage of DFC/T power plant.

v_i – The voltage magnitude at the inverter side in single-phase.

$v_{i,\,abc}$ - Three-phase voltage at the inverter side.

$v_{i,\,dq}$ - The voltage in *dq0*-frame at the inverter side.

$v_{idq,\,ref}$ - The voltage reference in *dq0*-frame.

v_g - The voltage magnitude at the grid side in single-phase.

ω_{ref} - The normal operating frequency.

ω_o - The output frequency of PLL.

δ_1 - The voltage phase angle at the inverter side

δ - The voltage phase angle at the grid side

$v_{g,\,abc}$ - Three-phase voltage at the grid side.

V_a, V_b, V_c - The input voltage of the PLL.

S_{err} - The error signal in the PLL.

V_{ref} - The voltage reference for the DC link voltage.

P_{ref}, Q_{ref} - Active and Reactive power reference.

$P_{FBK,}Q_{FBK}$ - The feedback active and reactive power.

P_L,Q_L - The active and reactive power of the load demand.

X_T - The inductance of transmission line.

ACKNOWLEDGMENTS

I would like to express my sincere gratitude to my advisor Dr. Kwang Y. Lee for all his guidance, support and patience in my graduate study and research.

Besides my advisor, I would like to thank the rest of my committee: Dr. Mack Grady and Dr. Paul Grabow for reviewing my thesis and giving valuable comments.

Many thanks to Dr. Wenli Yang for helping me start and guide my research patiently.

My sincere thanks also go to Dr. Mike Thompson for the help he gave in completing the Master's program. I am thankful for the education of Department of Electrical and Computer Engineering and Baylor University.

Last but not the least, I would like to thank my family in China, and thank my husband, for all their support and encouragement.

CHAPTER ONE

Introduction

1.1 Motivation

Distributed generation (DG) is a small-scale power generation, typically in the range of 3kW to 10,000kW, used to provide an alternative to or an enhancement of the traditional electric power generation. The small power plants in DG are categorized as photovoltaic, wind turbines, and fuel cells. However, wind turbines are constrained by the availability of wind and land, and photovoltaic are limited by the weather conditions. Fuel cell power plants, compared with other distributed energy sources, have become most promising for distributed generation due to their high efficiency, low emissions, flexible scalability, and fuel flexibility [1]-[3].

Fuel cells generate electricity through an electrochemical process, where the chemical energy stored in the fuels is converted into direct current (DC) electricity without combustion. The fuel cell power plant can achieve clean, quiet and efficient operations because the fuels can be utilized efficiently with the only by-productions of water and carbon dioxide. With high operational performance and flexible application capabilities, fuel cell power plant becomes a major source of distributed generation and possesses the ability of wide commercial applications.

When a fuel-cell power plant is connected to a distribution system, issues associated with power flow control and power quality must be resolved. Since the output voltage of a fuel-cell power plant is direct current (DC) and cannot be transmitted to the grid directly, an interface between fuel-cell power plant and the utility grid must be added

to provide voltage regulation, current regulation, power-flow control and power quality improvement. The interface is called power conditioning system (PCS).

An important issue in the simulation of a PCS is the simulation time step, which is very small for accurate modeling. Due to the high switching frequency of the devices, the simulation time step is on the order of μs (micro-second) or less for accurate switching simulation. As a result, a detailed model of a converter or inverter with its control switching signals dramatically decreases the simulation speed. This causes problems when we run a long time simulation. Therefore, effective averaged models of converter and inverter are utilized in this thesis. These averaged models can significantly improve the simulation speed and at the same time achieve sufficient accuracy.

1.2 Background

A fuel cell is a device that converts the chemical energy from a fuel into electricity through a chemical reaction with oxygen or some other oxidizing agent. Hydrogen is the most common fuel, but natural gas and methanol are the primary fuels that produce hydrogen. Fuel cells are different from batteries; they need a constant source of fuel and oxygen to run, but they can generate electricity continually for as long as these inputs are supplied. The by-products are water and carbon dioxide, which are totally pollution free. Fuel-cells have a variety of applications, such as in electric vehicles, airplanes, submarines, a stationary power source for home applications, cogeneration for office and factory, and distributed generation.

According to different electrolyte materials, there are mainly five types of fuel-cells. Some cells need pure hydrogen, and use additional equipment to purify the fuel.

Others can tolerate some impurities by running efficiently under higher temperatures [4]-[5].

Alkali fuel cells (AFC) operate on compressed hydrogen and oxygen. They generally use a solution of potassium hydroxide (chemically, KOH) in water as their electrolyte. Their efficiency is about 60% and their operating temperature is 90-100°C. The output range of cells is 10-100kW. Alkali cells were used in Apollo spacecraft to provide both electricity and drinking water [5].

Phosphoric Acid fuel cells (PAFC) use phosphoric acid as electrolyte. They can generate power at more than 40% efficiency and an operating temperature of 150-200°C. The output power is 400kW. The PAFC can tolerate a carbon monoxide concentration. They are being widely used in commercial buildings, airports and utility plants [5].

Proton Exchange Membrane fuel cells (PEMFC) work with a polymer electrolyte in the form of a thin, permeable sheet. They operate at relatively low temperature range from 50-100°C. Efficiency varies depending on different applications. For transportation, such as a fuel-cell car, vehicle or bus, they work at 60% efficiency. For a stationary plant, which is used for commercial, industrial and residential primary or backup power generation, the efficiency is 35%. The PEMFC ranges from 1kW-100kW. Due to their high power density and fast response, the most attractive applications are in the automotive industry and portable devices. However, costs for PEMFC are relatively high [5].

Molten Carbonate fuel cells (MCFC) use high-temperature compounds of salt (e.g., sodium or magnesium) carbonates (chemically, CO_3) as the electrolyte. They have a high efficiency of 45-50%. An MCFC operates at 600-700°C, so the natural gas fuel can

be reformed directly into hydrogen. This direct fuel cell (DFC) can generate 300kW to 3MW. Due to their high efficiency and high operating temperature, MCFC is used for base-load power generation [5].

Solid Oxide fuel cells (SOFC) use a hard, ceramic compound of metal (e.g., calcium or zirconium) oxides (chemically, O_2) as electrolyte. Their efficiency is approximately 60% and they operate at 700-1000°C. The output power ranges from 1kW to 2MW. At such high temperatures, the natural gas fuel can be reformed internally into hydrogen and waste heat can be recycled to make additional electricity [5].

1.2.1 Hybrid Direct Fuel Cell with Turbine Power Plant

The hybrid direct fuel cell (DFC) with a turbine (DFC/T) is used in this thesis. Integration of fuel cells with a gas turbine can greatly enhance the overall efficiency of the power plant. Compared to the conventional fuel conversion technologies, where fuel turns into a hydrogen-rich gas in an external fuel processor, the DFC reforms natural gas internally in the anode compartment with a reforming catalyst directly placed in the anode of the fuel cell [2].

Fig. 1 shows the structure of a DFC/T power plant [3]. The MCFCs are high-temperature fuel cells that operate at temperatures of 600°C and above. It can continuously generate power through an electrochemical process in the fuel-cell stack. Due to the high temperatures of MCFCs, the fuels are converted to hydrogen within the fuel cell itself by a process called internal reforming. The only by-products of a DFC/T power plant are water and carbon dioxide. Thus, it is environmental friendly with a higher efficiency than a conventional coal-based power plant. Due to these features, a

DFC/T power plant is one of the most promising distributed energy sources in the near future [6].

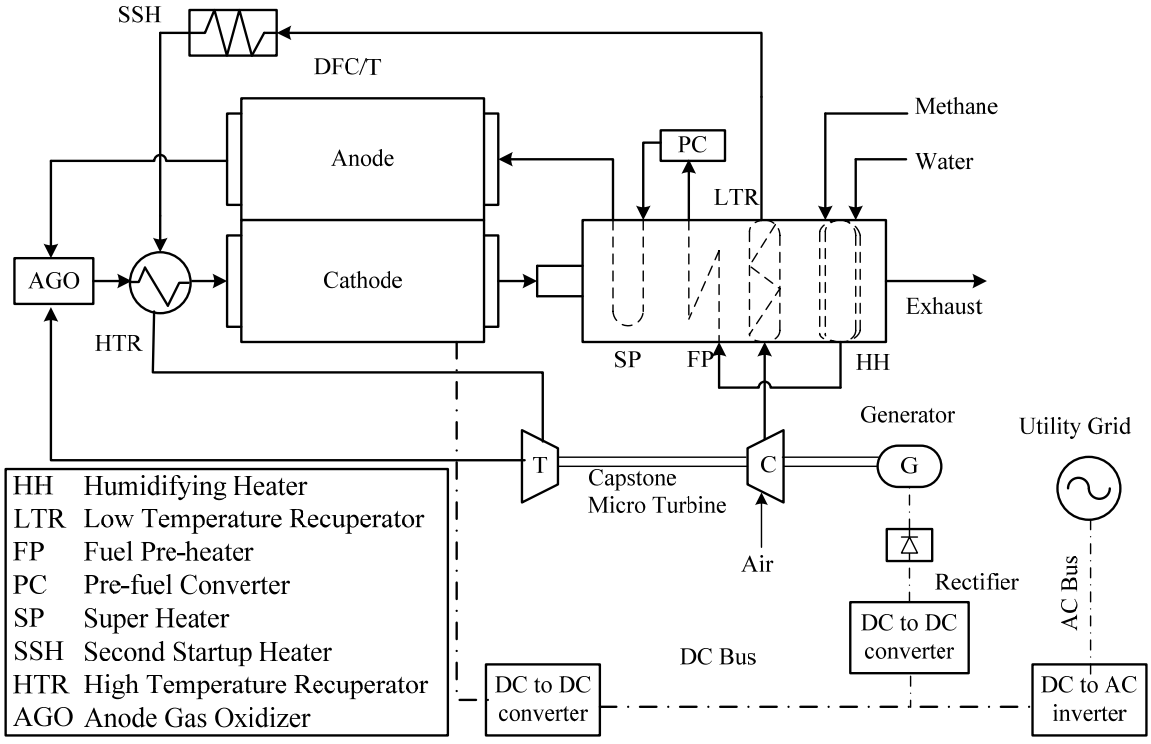

Fig. 1. Structure of Fuel Cell Stack with Turbine Power Plant.

The mathematical model of the DFC/T used in this thesis was first developed by Lukas, Lee and Ghezel-Ayagh [6], [7], and then Yang, Lee, Junker and Ghezel-Ayagh optimized the DFC/T model and developed an intelligent control system with a fuzzy fault diagnosis and accommodation system [3]. By integrating a micro-turbine into a fuel-cell power plant, the overall plant efficiency is expected to achieve 75% [3], [8]-[11].

1.2.2 Power Conditioning Systems

The power conditioning system (PCS) is an interface between a fuel-cell power plant and the utility grid. Fig. 2 describes the overall diagram of a fuel cell power plant

and PCS. Interfacing circuits of the PCS deal with electric power conversion and control using power semiconductor switches that operate at high speeds. The main tasks of a PCS are voltage regulation, current regulation, power flow control. With a PCS, high quality regulated power following load forecasting can be transmitted to the utility grid [12], [13].

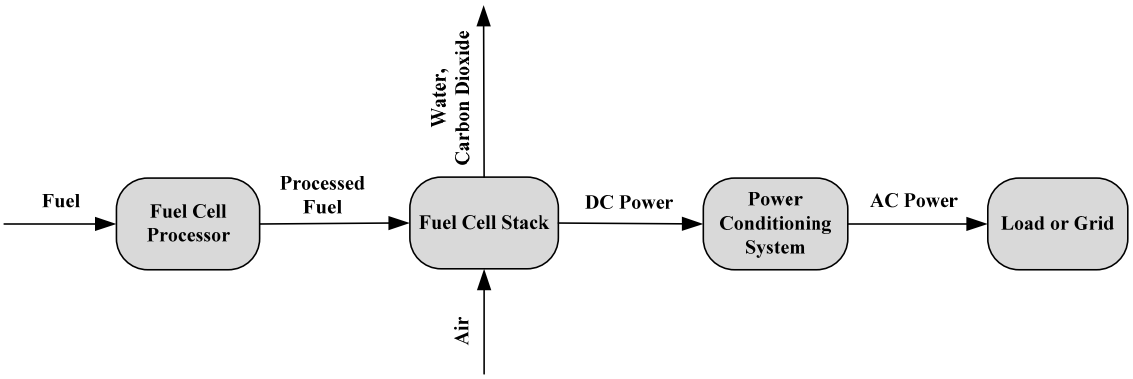

Fig. 2. The overall diagram of fuel cell power plant and PCS.

For fuel-cell generation systems, the PCS first regulates the DC voltage source before converting it to alternating current (AC) for transmission. Fig. 3 shows the overall structure of the PCS. As shown in figure, a PCS consists of a DC/DC converter and a DC/AC inverter and LCL filter. The output power generated by fuel cell power plant is regulated and controlled by the PCS. The converter is to adapt the output voltage of fuel cell to the desired DC voltage because the DC output voltage of fuel cell power plant is not stable. To stabilize the DC bus voltage and reduce ripples of the DC bus voltage, a large capacitor is place between converter and inverter. For the inverter, the function is to convert DC power into AC with a desired magnitude and frequency. The active and reactive power delivered to the utility grid can be controlled according to the load demand through PQ controller.

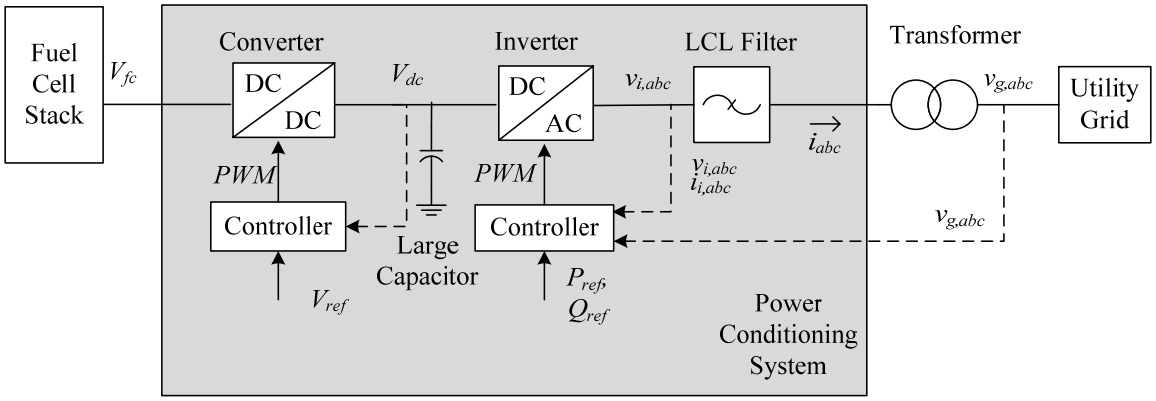

Fig. 3. The overall structure of the PCS.

1.3 Recent Research and Achievements

There has been a considerable amount of research done to explore the use of the detailed and averaged model of a PCS. The general structure and basic principles of the PCS have been investigated, and different power conditioning circuit topologies were introduced in [12], [13]. The state space averaged model of the converter and averaged switch model of the inverter have been developed respectively in [20], [21]. However, a fully operational averaged model of the PCS has not been developed to connect to the utility grid. Therefore, I have developed an averaged model of the PCS and it is described in Chapters 2 and 3.

1.4 Thesis Organization

The averaged model of a DC/DC converter and a DC/AC inverter is described in Chapters 2 and 3, respectively. Chapter 4 gives the power flow control through current and voltage regulation. Chapter 5 presents the phase locked loop design and Chapter 6 shows the simulation results of the DC bus voltage and the power flow control. Conclusions are drawn in Chapter 7.

CHAPTER TWO

Averaged Model of DC/DC Converter

2.1 Introduction to DC/DC Converter

The output voltage of a DFC/T power plant is DC, and is low when it is connected to an inverter. Moreover, the output DC voltage varies over a wide range. Thus, a DC/DC converter is needed to regulate the DC bus voltage so that it is stable.

There are three types of DC/DC converters, a Buck converter, a Boost converter and a Buck-Boost converter. A Buck converter is a step-down converter where the output voltage is lower than the input voltage. A Boost converter is a step-up converter where the output voltage is greater than its input voltage. A Buck-Boost converter has an output voltage that is either greater than or less than the input voltage based on the switching duty-ratio. A converter is composed of an inductor, a capacitor, a switching device and a diode. The switching device, such as a metal oxide semiconductor field effect transistor (MOSFET) or an insulated gate bipolar transistor (IGBT), can be either ON or OFF; and it is directly controlled by a pulse width modulation (PWM) wave generator [14].

2.1.1 PWM and Duty Cycle

The PWM is a commonly used technique for controlling power electronics devices and motor drives. The main advantage of a PWM is that power loss in the switching devices with a high frequency is very low. There is practically no current while the switch is OFF, and there is almost no voltage drop across the switch when it is ON. The PWM switching frequency has to be much faster than what would affect the load,

which is to say the device that uses the power. Typically switching frequency is range from few kilohertz (Hz) to tens of kHz for the power electronics or a motor drive. Fig. 4 shows the basic principles used to generate a PWM wave. In the figure, the input sinusoidal control signal is compared with the internal saw-tooth wave, which is generated at the switching frequency. If the input signal is larger than the saw-tooth wave, then the rectangle output PWM wave is in the high state (*amplitude* = 1). Otherwise, the rectangle output signal is in the low state (*amplitude* = 0). The high state is used to close the switching device and the low state is used to open the switching device.

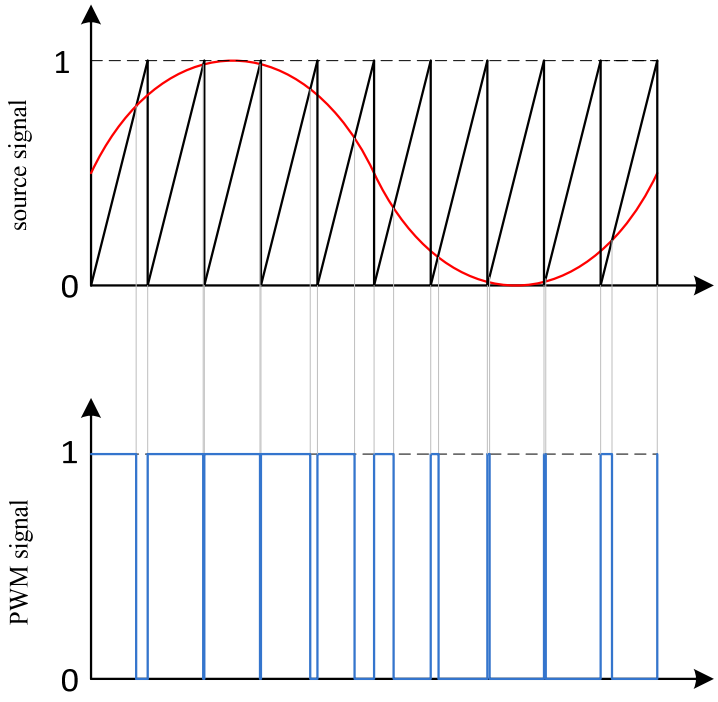

Fig. 4. PWM Signal Generator

The duty ratio is defined as follows in one period:

$$D = \frac{\tau}{T} \tag{2.1}$$

where τ is the time when output is in the high state during one time period and *T* is the width of the one time period. Thus, the duty cycle, *D,* is a decimal value between 0 and 1.

2.2 The Averaged Model of Buck-Boost Converter

Because high frequency switches are used in power electronic circuits, an important issue for simulation studies is the choice of the simulation time step. Typically, the simulation time step needs to be in the order of μs or less for an accurate switching simulation. As a result, a detailed model of a converter with its switching control signal decreases the simulation speed considerably. Especially, it is impossible to carry out long time simulation studies such as several hours. Thus, an effective average state space model of converter is used in this chapter to improve the simulation speed and to achieve the desirable accuracy. The high frequency of PWM signal isn't necessary to use when the average state space model of converter is applied instead of the detailed model.

As we can see in Fig 5, the output voltage of the fuel-cell stack is unstable and low compared with the DC bus voltage, which is 480V. It represents of 42 day simulation data, which means that the model runs for 42 days. Thus, the output voltage should be regulated with the desired DC voltage before they are connected to the inverter and transmitted to the grid. The output voltages of the fuel-cell stack varies from 270V to 360V. Since the DC bus voltage is supposed to be 480V, Buck-Boost converter is adopted here, because of the wide range of the input voltage to be regulated [3].

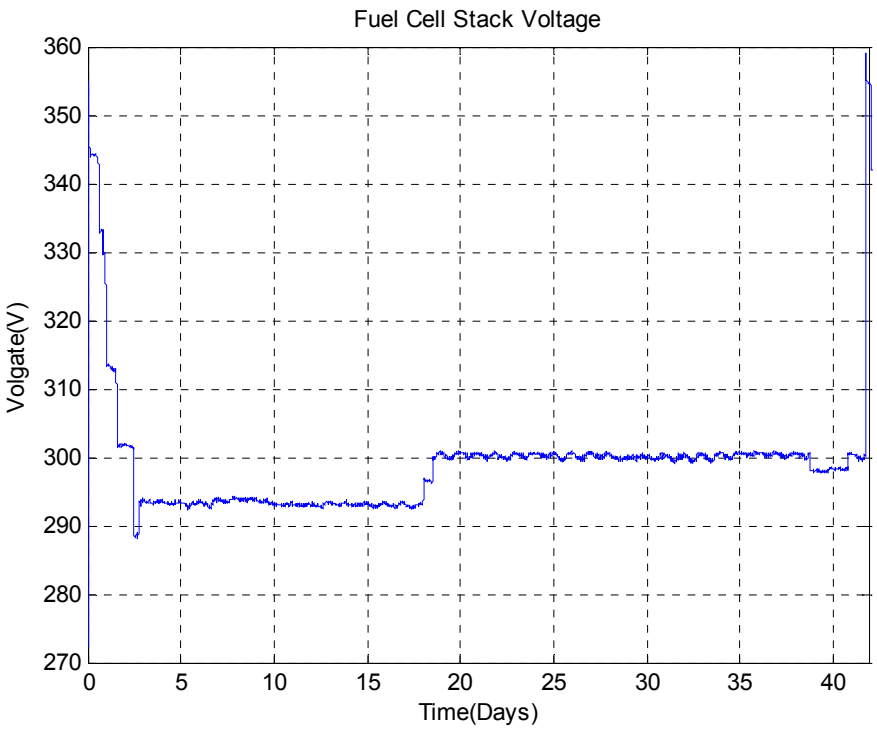

Fig. 5. Fuel Cell Stack Output Voltage.

The topology of the Buck-Boost circuit is shown in Fig. 6, where V_{fc} is the output voltage of the fuel-cell stack, V_{dc} is the DC link voltage, L is the inductance with its equivalent series resistance (ESR) R_L, C is the capacitance, and R is the equivalent load. The switching device S, directly controlled by the PWM signal, controls the whole circuit to be either buck type or boost type.

According to the different positions of the switching device S, there are two modes of the circuit as shown in Fig 7 and Fig 8. When the switch is ON, the inductor is charging and the capacitor is discharging. The current in the inductor would then increase and the inductor voltage would be equal to the input voltage, transferring the energy from the input voltage source to the inductor. The output voltage equals the capacitor voltage, transferring the energy from the capacitor to the load. When the switch is OFF, the

inductor is discharging and the capacitor is charging. The inductor current flows through the load and the diode, transferring the energy stored in the inductor to the capacitor and the load [15].

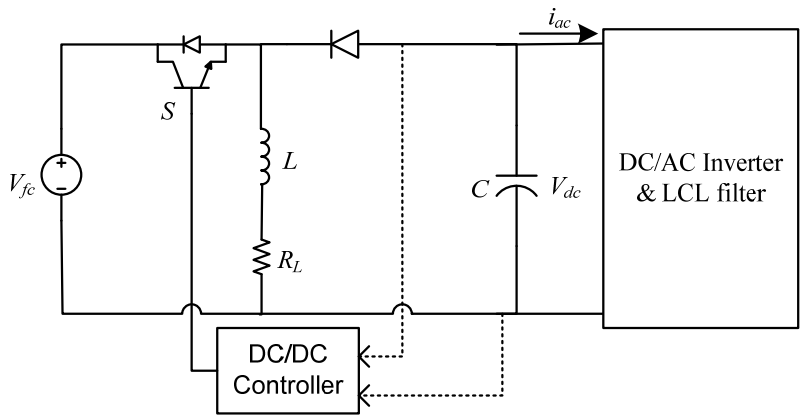

Fig. 6. Topology of Buck-Boost DC/DC Converter.

When the switch is ON and the diode is OFF as shown in Fig. 7, the state- space representation of the main circuit can be written as

$$\dot{x} = A_1 x + B_1 V_{fc} \tag{2.2}$$

$$\dot{V}_o = C_1 x \tag{2.3}$$

where $x = \begin{bmatrix} i_L & V_o \end{bmatrix}^T, A_1 = \begin{bmatrix} \frac{-R_L}{L} & 0 \\ 0 & \frac{-1}{RC} \end{bmatrix}, B_1 = \begin{bmatrix} \frac{1}{L} \\ 0 \end{bmatrix}, C_1 = \begin{bmatrix} 0 & 1 \end{bmatrix}.$

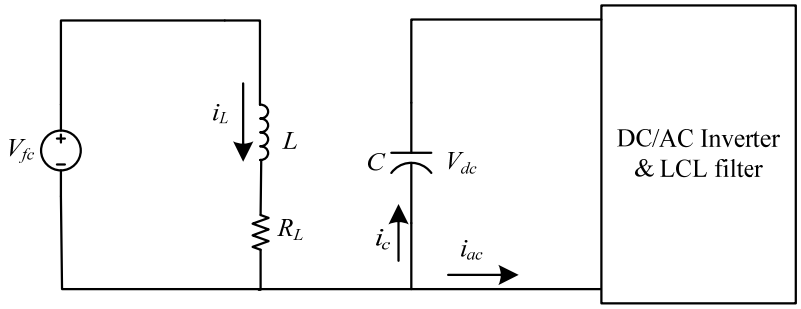

Fig. 7. Case for the switch-on condition.

When the switch is OFF and the diode is ON as shown in Fig. 8, the state-space representation of the main circuit can be written as

$$\dot{x} = A_2 x + B_2 V_{fc} \tag{2.4}$$

$$\dot{V}_o = C_2 x \tag{2.5}$$

where $x = \begin{bmatrix} i_L & V_o \end{bmatrix}^T, A_2 = \begin{bmatrix} \frac{-R_L}{L} & \frac{-1}{L} \\ \frac{1}{C} & \frac{-1}{RC} \end{bmatrix}, B_2 = \begin{bmatrix} 0 \\ 0 \end{bmatrix}, C_2 = \begin{bmatrix} 0 & 1 \end{bmatrix}.$

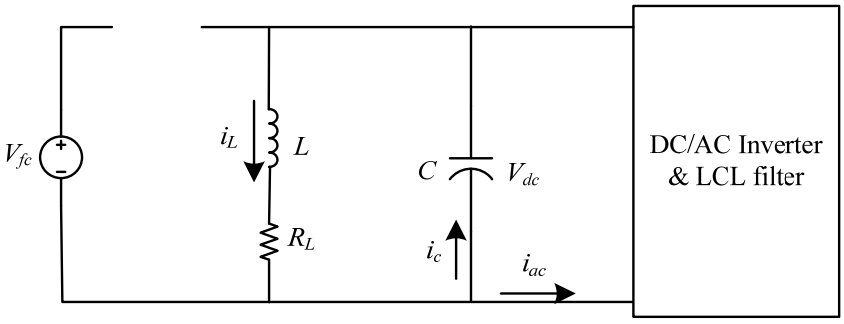

Fig. 8. Case for the switch-off condition.

The average state-space model of the Buck-Boost converter is

$$\dot{x} = Ax + BV_{fc} \tag{2.6}$$

$$\dot{V}_o = Cx \tag{2.7}$$

where $x = \begin{bmatrix} i_L & V_o \end{bmatrix}^T, A = \begin{bmatrix} \frac{-R_L}{L} & \frac{-(1-d)}{L} \\ \frac{(1-d)}{C} & \frac{-1}{RC} \end{bmatrix}, B = \begin{bmatrix} \frac{d}{L} \\ 0 \end{bmatrix}, C = \begin{bmatrix} 0 & 1 \end{bmatrix}.$

2.3 Converter Controller Design

Before connecting a fuel cell power plant to a grid, a DC/DC converter is needed to regulate the fuel cell output voltage and adapt it to the desired voltage to be supplied to the DC/AC inverter. The duty ratio of the converter in the proposed averaged model will be a decimal value between 0 and 1.

The configuration of the controller for converter is shown in Fig. 9. A conventional PI controller is adapted here to achieve the duty ratio. The output of converter V_{dc} is compared with the desired output V_{ref}, which is 480V. The difference will go through the PI controller to achieve the duty ratio of the converter [16]-[18].

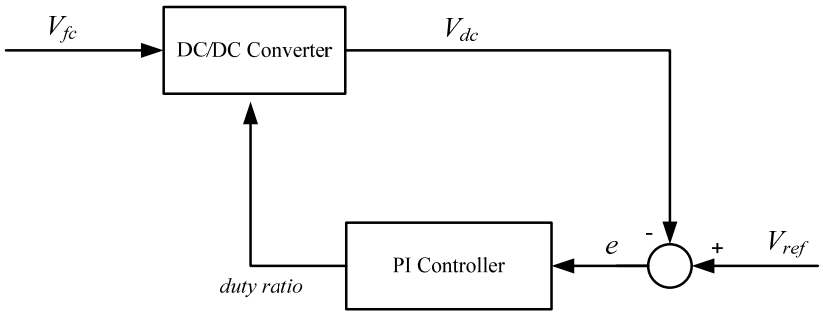

Fig. 9. The scheme of the converter controller.

Fig. 10 shows the block diagram for the converter circuit with the controller when it is linearized around its operating point. In the figure, the controller is implemented by a PI controller.

The transfer function for each block in the block diagram is written as

$$G_c(s) = \frac{K_d s + K_i}{s} \tag{2.8}$$

$$T(s) = \frac{V_{fc}}{(1-D)^2}\left(1 - s\frac{DL}{R(1-D)^2}\right)\frac{1}{\frac{LC}{(1-D)^2}\left(s^2 + \frac{s}{RC} + \frac{(1-D)^2}{LC}\right)} \tag{2.9}$$

$$D = \frac{V_{dc}}{V_{dc} + V_{fc}} \tag{2.10}$$

where D is the rated duty ratio of the switch, L is the inductance, C is the capacitor, R is the equivalent resister of the load, V_{fc} is the average value of the input voltage and V_{dc} is the average value of the output voltage.

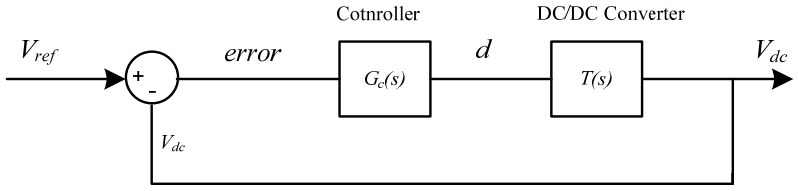

Fig. 10. Block diagram of the converter control.

2.4 Parameters for Buck-Boost Converter and Control System

The parameters of the Buck-Boost converter and control system should be chosen appropriately to meet the design requirements of the DC/DC converter. The regulated output voltages of two DC/DC Buck-Boost converters are 480V; however, they still have some small ripples due to switching patterns and storage devices. Based on the specific current ripples and voltage ripples, the choice of the inductor and capacitor in the Buck-Boost converter are given by the following equations [14]:

$$L = \frac{V_{fc} D T_s}{\Delta i_L} \tag{2.11}$$

$$C = \frac{I_o D T_s}{\Delta V_{dc}} \tag{2.12}$$

where V_{fc} is the voltage of fuel-cell stack, D is the average duty ratio as calculated in above equation, T_s is the one period of the PWM signal, that is, $T_s=1/f_s$, with f_s as the switching frequency, and Δi_L is the inductor current ripples in ampere (A), which is less than 3% of the inductor current. Furthermore, I_o is the average output current and ΔV_{dc} is the voltage ripples in volt (V), which is less than 1% of the DC link voltage. According to the design requirements, the current ripple limit and voltage ripples limit must be defined. Then with these two equations, the inductor and the capacitor can be calculated. The controller parameters can be adjusted from the values obtained through the above design procedure based on the simulation study. The parameters of DC/DC converter and control loop are given in Table 1.

Fig. 11 shows the close-loop bode diagram for the Buck-Boost converter control system with PI controller. The gain margin of the close-loop is 8.85dB and the phase margin 14.6º, which implies that the proposed converter control system is stable with small signal disturbances because of the positive phase margin [19].

Table 1: Parameters of DC/DC Converter and Control System.

Parameters	Value
L	0.5mH
C	86mF
R_L	0.02mΩ
R_{eq}	1.3553Ω
K_d	0.0002
K_i	0.001
V_{dc}	480V
D (average value)	0.6154
f_s	5kHz
Δi_L	3%
ΔV_{dc}	1%

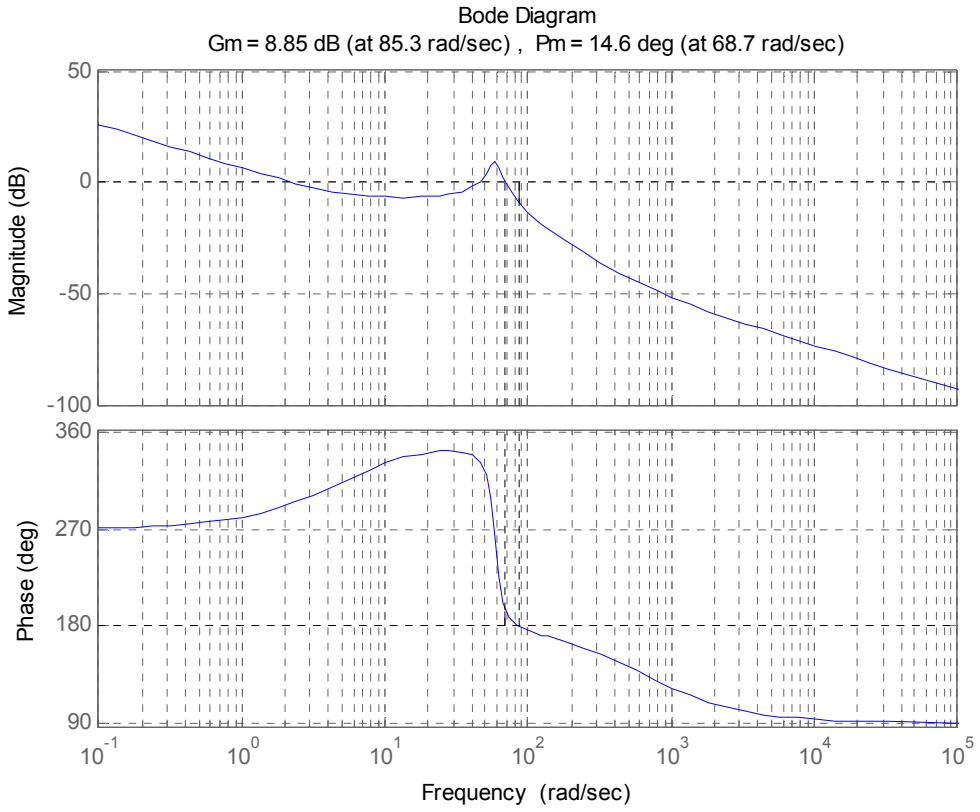

Fig. 11. Bode Diagram of the Control System for Buck-Boost Converter.

CHAPTER THREE

Averaged Model of Three-phase Inverter

3. 1 Introduction to Voltage Source Inverters

An inverter is an electrical power converter that changes DC to AC; the converted AC can be at any required voltage and frequency with the use of appropriate transformers, switching, and control circuits. It can convert the DC voltage sources, such as photovoltaic, fuel-cell or batteries, into AC voltage to be utilized or transmitted. Depending on the type of the supply source and the related topology of the power circuit, there are two types of inverters, a voltage source inverter (VSI) and a current source inverter (CSI) [15]. The circuit topology of a typical 3-phase 6-switch PWM VSI is shown in Fig.12.

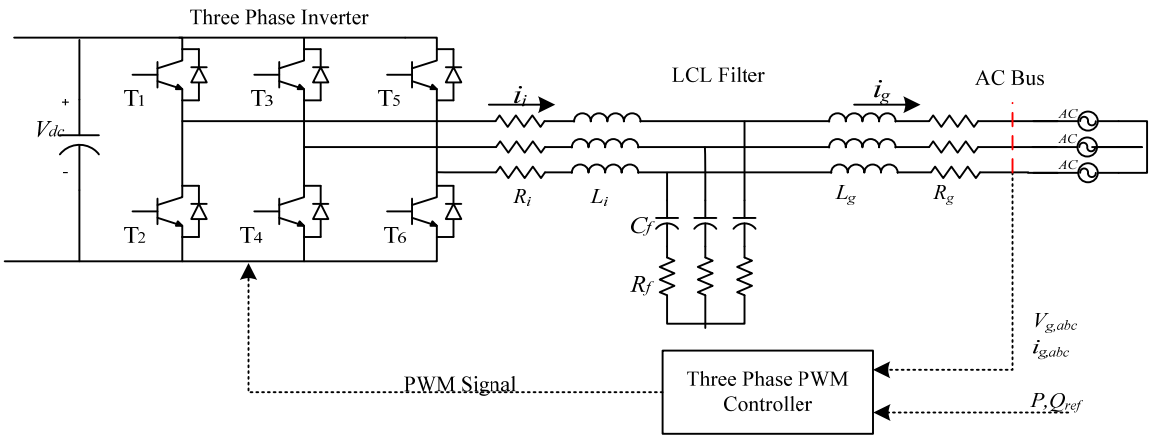

Fig. 12. Three Phase Full-Bridge Inverter.

As shown in Fig. 12, there are three arms in the inverters, one for each phase. Each arm consists of two power electronic switches. T_1 to T_6 are six switching devices

that are directly controlled by a PWM signal to be either ON or OFF. A sinusoidal pulse-width-modulation (SPWM) is one of the modulation schemes used to control and shape the VSI output voltages.

3.1.1 Three-Phase SPWM Wave

In order to control the magnitude, phase angle and frequency of the output voltage on the DC side of VSI, SPWM is used to generate appropriate switching pulses to control the six switches in the inverter as shown in Fig. 13. The three-phase SPWM wave is the rectangular wave that is generated by the three-phase SPWM generator. The three sinusoidal waves are the balanced sinusoidal control voltage signals for three-phase. They are compared with the internal triangular wave to generate SPWM in each phase. The wave is generated at the switching frequency f_s, normally 5 to 10 kHz, which is generally much higher than the frequency of the control voltage and is called the carrier frequency.

Each pair of switching devices, T_1 - T_2, T_3 - T_4, and T_5 - T_6, comprise a switching arm. In one time period, only one switching device is closed in one arm. See phase (*a*) in Fig. 13, for example. If the control signal voltage is larger than the triangular carrier signal, then T_1 is ON and T_2 is OFF. On the contrary, if the control signal voltage is less than the carrier signal, then T_1 is OFF and T_2 is ON. For phases *b* and *c*, the operation is exactly the same as phase *a*.

The output voltage, depending on the switching pattern of the SPWM wave, can be either positive or negative, and generates the AC source voltage. The difference in phase angle depends on the SPWM wave.

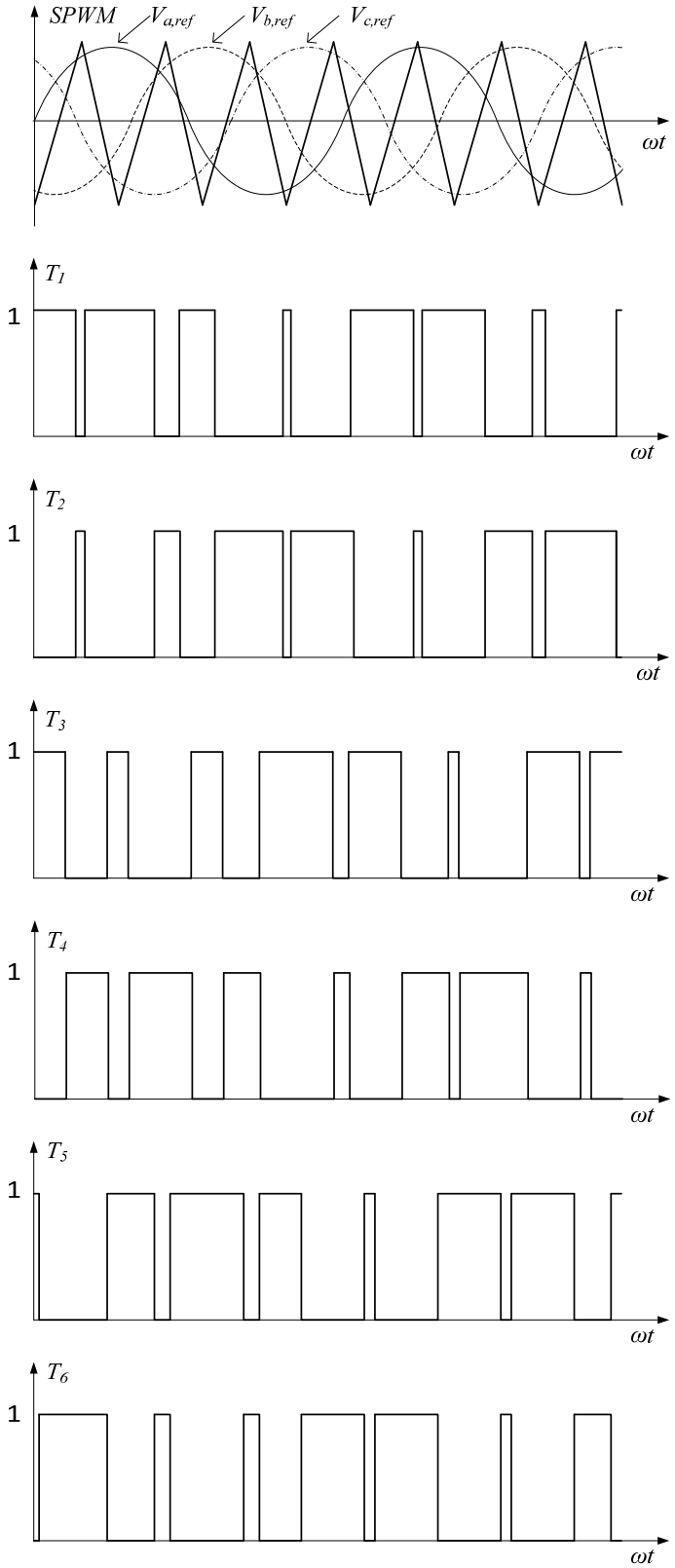

Fig. 13. Three-Phase SPWM Wave.

3. 2 The Averaged Model of Three-Phase Inverter

The switching model of the inverter, as shown in Fig. 12, has two limitations. First, the switching model is inefficient because it takes a long time to simulate. Typically, it takes more than 10 minutes to run several seconds of simulation time. Second, it cannot perform small-signal analysis due to its discrete behaviors [20]. The averaged model can overcome these limitations. The circuit averaging model of the inverter uses in Fig. 14, and shows an averaged model of each one of the inverter arms, which can be represented by controlled voltage and current sources with averaged switching duty cycles [21].

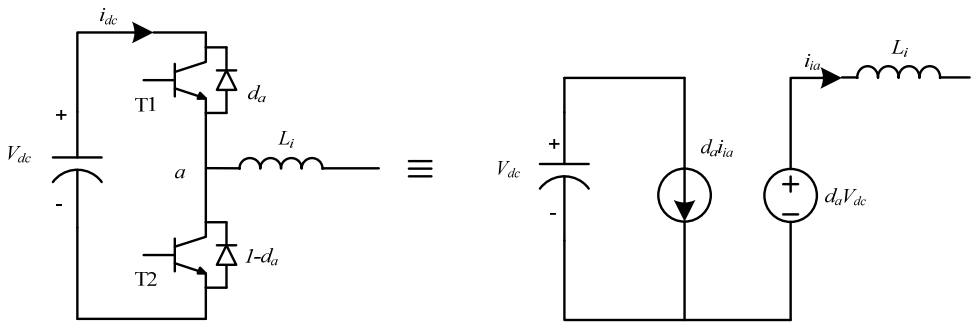

Fig. 14. Averaged equivalent circuit of an inverter arm.

In Fig. 14, d_a is the duty cycle of the upper switch of the inverter arm in a switching period. The average values during a switching period of the voltage across and current through the lower switch are represented by duty cycle as shown in Fig. 14. The current flowed into the point *a* in the left of Fig. 14 is represented by multiplying the duty cycle with the inductor current. The voltage at the point *a* is calculated by multiplying the duty cyle with the DC bus voltage as shown in Fig. 14. By averaging the three inverter

arms in swiching model shown in Fig. 14, the whole averaged model of the inverter is obtained in Fig. 15. According to this scheme, the set of equations is derived [21]:

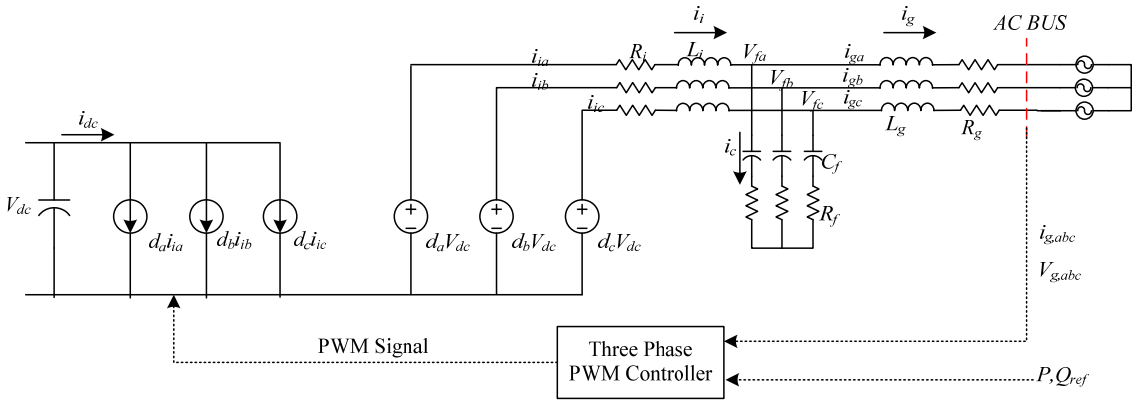

Fig. 15. Averaged equivalent circuit in the three-phase VSI.

$$\begin{cases} \dfrac{di_{ia}}{dt} = \dfrac{1}{L_i}[-R_i i_{ia} - V_{fa} + d_a V_{dc}] \\ \dfrac{di_{ib}}{dt} = \dfrac{1}{L_i}[-R_i i_{ib} - V_{fb} + d_b V_{dc}] \\ \dfrac{di_{ic}}{dt} = \dfrac{1}{L_i}[-R_i i_{ic} - V_{fc} + d_c V_{dc}] \end{cases} \tag{3.1}$$

$$\begin{cases} i_{ia} = i_{ga} + i_{fa} \\ i_{ib} = i_{gb} + i_{fb} \\ i_{ic} = i_{gc} + i_{fc} \end{cases} \tag{3.2}$$

$$\begin{cases} i_{fa} = \dfrac{d(V_{fa} - R_f i_{fa})}{dt} \\ i_{fb} = \dfrac{d(V_{fb} - R_f i_{fb})}{dt} \\ i_{fc} = \dfrac{d(V_{fc} - R_f i_{fc})}{dt} \end{cases} \tag{3.3}$$

$$\begin{cases} \dfrac{di_{ga}}{dt} = \dfrac{1}{L_g}[-R_g i_{ga} - V_{fa} + e_A] \\ \dfrac{di_{gb}}{dt} = \dfrac{1}{L_g}[-R_g i_{gb} - V_{fb} + e_B] \\ \dfrac{di_{gc}}{dt} = \dfrac{1}{L_g}[-R_g i_{gc} - V_{fc} + e_C] \end{cases} \tag{3.4}$$

3. 3 Simplified Model of Three-Phase VSI

A detailed model of the inverter which consists of power electronic switches which has high frequency. Due to the high frequency of the switching devices, the simulation time step is made very small. As a result, it isn't suitable for long-time simulation. Thus, a simplified inverter model is required to use [15],[29],[30].

The averaged models of a DC/DC converter is presented in equations (2.6) and (2,7), and a DC/AC inverter are presented in Fig. 15, respectively. However, when they are combined together to become a power conditioning unit, the current flow from converter to inverter should be known. Since we assume that there are no power losses from converter to inverter, the output power of the converter is equal to the input power of the inverter.

Fig. 16 shows how the simplified inverter works. Here, V_{dc}, I_{dc} stand for the output voltage and current of the DC bus, respectively, d_a(t), d_b(t) and d_c(t) are the three-phase duty cycles of the inverter which will be presented in the next section; and V_a(t), V_b(t) and V_c(t) are the three-phase output voltages of the inverter [15].

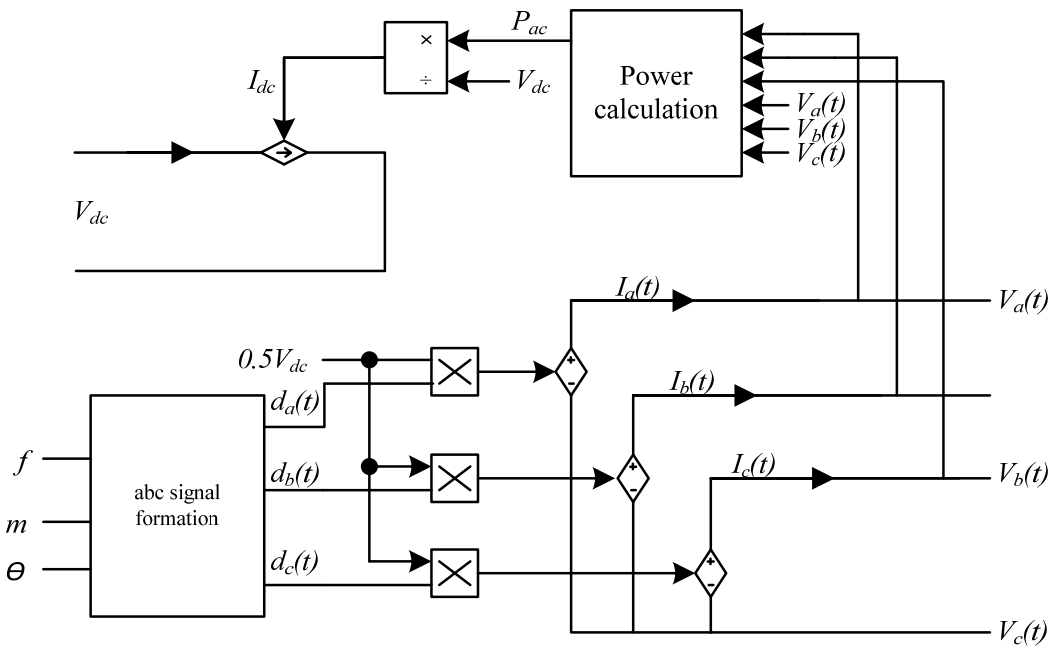

Fig. 16. Simplified model of the inverter.

The power P can be calculated as

$$P = I_a(t)V_a(t) + I_b(t)V_b(t) + I_c(t)V_c(t) \tag{3.5}$$

where I_a(t), I_b(t) and I_c(t) are the three-phase instantaneous values of the inverter current, P is the three-phase instantaneous power which is constant for balanced system.

Since there is no power loss, input power is equal to the output power of the inverter. Thus, the output current of DC bus can be written as

$$I_{dc} = P \div V_{dc} \tag{3.6}$$

The relationship between converter and inverter with respect to current can easily be derived. The output current of the converter is the sum of the current of the dc bus capacitor plus the inverter input current I_{dc}, as shown in Fig. 16.

CHAPTER FOUR

Power Flow Control of Grid-connected Fuel Cell Power Plant

4. 1 Introduction

When the output power of a fuel-cell power plant is transmitted to the grid, the output of voltage magnitude and phase angle should be regulated based on the desired voltage magnitude and phase angle. By using the control of the inverter, not only DC bus voltage is converted to a desired AC voltage, but also implement the power flow control. To meet the demands of the utility grid in different operation modes, the controller of the inverter needs to be designed properly to control the real and reactive power flow from the fuel cell power plant to utility grid. This chapter will discuss the power flow control by controlling the inverter in the grid-connected operation mode.

In the grid-connected operation mode, the main function of a fuel cell power plant is to control the real and reactive power, where the real power reference can be taken from the grid energy management controller. There are several types of controllers for the inverter. For example, the real and reactive power can be controlled through current regulation or through voltage regulation.

4. 2 Power Flow Control through Current Regulation

With power flow control through current regulation, if both real and reactive power flow is to be controlled, then the real power control loop can generate the synchronous frame d-axis reference current (i_d) and the reactive power control loop can produce the q-axis current (i_q). Generally, the unity power factor should minimize the

inverter power losses. As a result, a null reference for the q-axis current is chosen [21], [22].

$$i_d = \frac{2}{3} \cdot \frac{PV_q - QV_d}{V_d^2 + V_q^2} \tag{4.1}$$

$$i_q = \frac{2}{3} \cdot \frac{PV_d + QV_q}{V_d^2 + V_q^2} \tag{4.2}$$

Fig. 17 shows the scheme for the current control structure. The inverter output currents are regulated to the given current references, so the reference current on the d-axis and on the q-axis, i_{dref} and i_{qref}, are calculated using equations (4.1) and (4.2). The measured inverter output currents in the three-phase form are transformed onto the d-q axis current through an abc/dq transformation, i.e., the *Park* transformation. The difference between reference and actual output current for the d-axis and the q-axis is calculated. The duty cycle is achieved by adding the decoupling terms K_d and K_q with the value calculated by the difference going through the PI controller. The decoupling gain K_d and K_q can be calculated by using the equations (4.3) and (4.4):

$$K_{qd} = \frac{-\omega(L_1 + L_2)}{V_{dc}} \tag{4.3}$$

$$K_{dq} = \frac{\omega(L_1 + L_2)}{V_{dc}} \tag{4.4}$$

Compared to the power control through current regulation, the voltage regulation is more sensitive to the line impedance between the fuel cell and the grid, and thus a small line impedance will cause significant power flow even with a slight variation of the fuel cell output voltage. However, voltage regulation is similar to the voltage control strategy

that can be used in islanding grid operation employed by the *P*-ω and *Q*-*V* droop methods. Using a similar control strategy in different operation modes enhances smooth transients between operation modes. Therefore, the voltage regulation control was chosen as the inverter in this thesis [22].

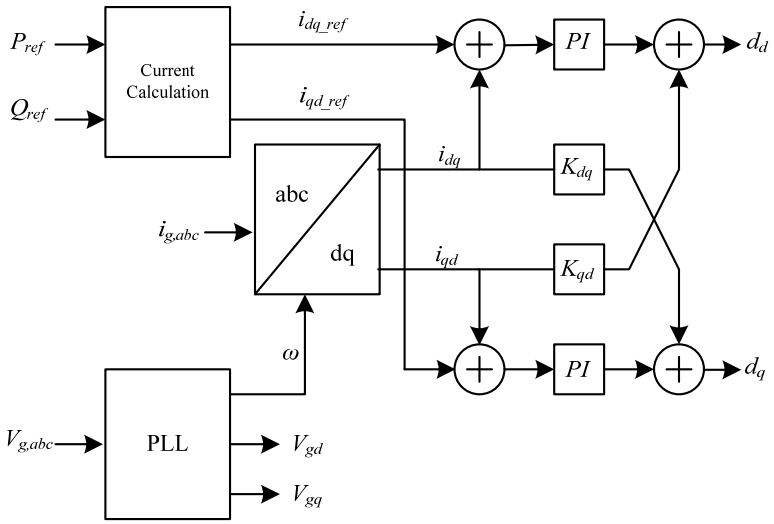

Fig. 17. Block Diagram of Current Control.

4. 3 Power Flow Control through Voltage Regulation

Power flow control through voltage regulation is related to the real and reactive power flows between the inverter output voltage and the grid input voltage. Consider a two-node circuit as shown in Fig. 18. Typically, the line impedance ($Z=R+jX$) is represented by a transformer and/or LC filter. Then, the real and reactive power flows are computed as follows [22]-[24], [31]:

$$P = \frac{V_g}{R^2 + X^2}(R(V_1 \cos\delta - V_g) + XV_1 \sin\delta) \tag{4.5}$$

$$Q = \frac{V_g}{R^2 + X^2}(RV_1 \sin\delta - X(V_1 \cos\delta - V_g)) \tag{4.6}$$

where V_1 and V_g are the voltage magnitudes of inverter and grid, respectively, and δ is the phase angle difference between the two voltages.

Due to the mainly inductive line or filter with a high X/R ratio, the resistance may be neglected. Typically, the phase angle difference δ is small, thus it can be assumed that $sin(\delta) \approx \delta$ and $cos(\delta) \approx 1$. As shown in Equations (4.5) and (4.6), we can conclude that the flow of real power P is proportional to the phase angle δ and the flow of reactive power Q is proportional to the voltage magnitude difference (V_1-V_g) due to a high X/R ratio.

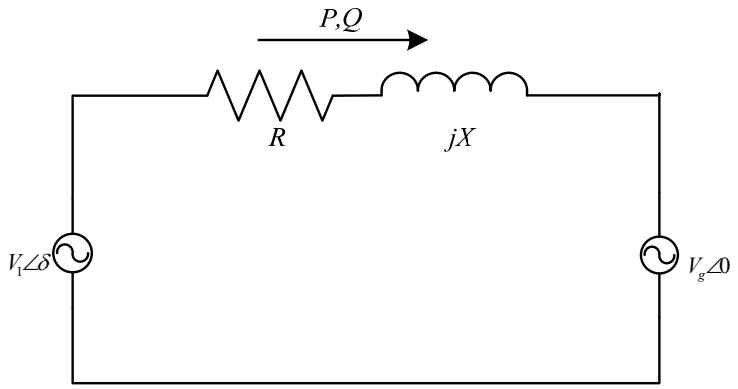

Fig. 18. Power flow between two sources.

According to the above relationship, the output real power can be controlled by regulating the output voltage phase angle δ, and the output reactive power can be controlled by regulating the output voltage magnitude [32]-[35].

As shown in Fig. 19, to achieve power flow control, several parameters are required, including the desired real and reactive power, the feedback real and reactive power that represent the output power of inverter. By using the P-ω and Q-V relationship, the duty cycle of the inverter can be calculated as shown in Fig. 19, where P_{ref} and Q_{ref} are the real and reactive power demands of the utility grid, and P_{Fbk} and Q_{Fbk} are the output real and reactive power of inverter. The difference between the reference and the actual

power is the conventional PI controller input. Since the reference of the voltage magnitude and voltage phase are achieved, then the duty cycle could be calculated according to the following equation:

$$d(t) = 0.5 \cdot V \sin(\omega t + \phi) \tag{4.7}$$

where V is the voltage magnitude, ϕ is the voltage phase angle, and ω is the frequency of the grid voltage [21],[24],[25],[28].

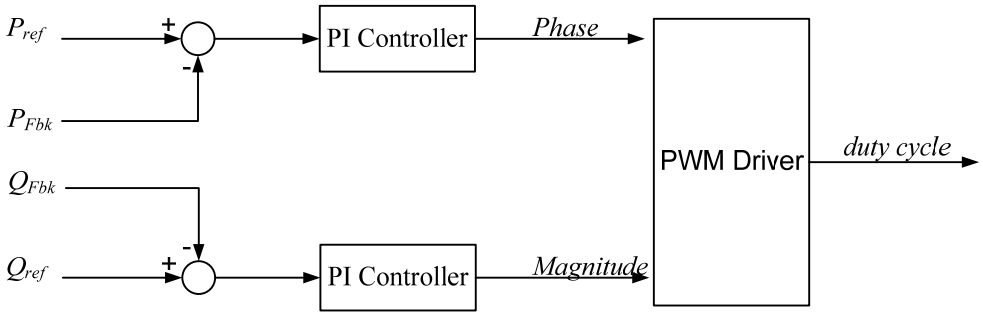

Fig. 19. Scheme of PQ controller for inverter.

4. 4 Fuel-Cell Power Plant Connected to the Grid

When a fuel-cell power plant is connected to a power grid, it is necessary to calculate the power flow to determine the real and reactive power of the fuel-cell power plant. The most common formulation of the power flow problem requires that all input variables (PQ at loads, PV at generators) are specified as deterministic values. There are 3 types of buses in power flow and they are classified as:

1. PQ bus - the real power P and reactive power Q are specified. It is also known as Load Bus.
2. PV bus – the real power P and the voltage magnitude V are specified. It is also known as Generator Bus.
3. Slack bus – used to balance the real and reactive power in the system. It is also known as the Swing Bus or Reference Bus.

Consider fuel cell power plant as a generator in the power system as shown in Fig. 20. Because the bus connected with the fuel-cell power plant can be viewed as a PV bus, the reactive power and voltage phase angle can be calculated by the power flow. Power flow control could then be implemented using the reference values calculated from the power flow. Tables 2 and 3 shows the bus and line input data in Fig. 20.

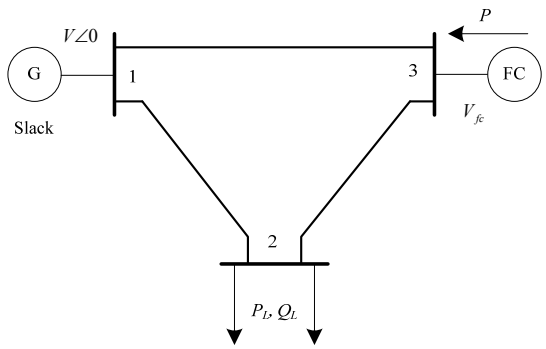

Fig. 20. Fuel Cell Power Plant integrated into Grid.

Table 2: Bus input Data.

Variables	Bus1	Bus2	Bus3
Real Power (kW)	-	120	100
Reactive Power (kVAR)	-	12	-
Voltage Magnitude (p.u)	1.025	-	1.03
Voltage Phase Angle (p.u)	0	-	-

Table 3: Line input Data.

Bus-to-Bus	R(p.u)	X(p.u)
1-2	0	0.025
1-3	0	0.05
2-3	0	0.025

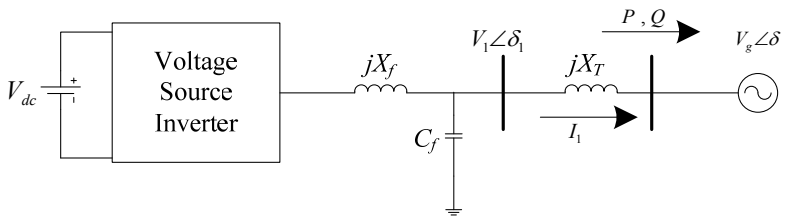

Fig. 21. VSI connected to Grid.

Fig. 21 shows the simplified structure of a fuel cell power plant as a generator connected to power system. The bus connected to the fuel cell is a PV bus where P and V_g are specified. The internal values are computed as the follows:

$$\bar{I}_1 = \frac{P - jQ}{\bar{V}_g} \tag{4.8}$$

$$\bar{V}_1 = \bar{V}_g + jX_T \bar{I}_1 \tag{4.9}$$

$$\bar{V}_1 = V_1 \angle \delta_1 \tag{4.10}$$

$$\bar{V}_g = V_g \angle \delta \tag{4.11}$$

By using the power flow, four variables (P, Q, V, and δ) can be determined. Thus, real and reactive power references are achieved from the power flow, and the duty cycle, control signal of the inverter can be calculated according to the PQ controller in Fig. 19.

CHAPTER FIVE

Phase Locked Loop

5. 1 Introduction to Phase Locked Loop

A phase locked loop is a control system that generates an output signal whose phase is related to the phase of an input "reference" signal. It consists of a variable frequency oscillator and a phase detector. The phase locked loop (PLL) was originally described in [25] and is widely employed in radio, telecommunications, computers and other electronic applications. It can be used to recover a signal from a noisy communication channel, generate stable frequencies at a multiple of an input frequency (i.e., frequency synthesis), or distribute clock timing pulses in digital logic designs such as microprocessors. Since a single integrated circuit can provide a complete PLL building block, the technique is widely used in modern electronic devices, with output frequencies ranging from a fraction of a Hz up to many Giga Hz.

In the area of power electronics, the PLL technique has been adopted for the speed control of electric motors, as well as synchronizing utility voltages and the control of currents or voltages in utility interface operations [26]. Thus, the main use of PLL used in this thesis is to synchronize the output voltage of VSI with the utility voltage when the fuel-cell power plant is connected to a grid.

5. 2 Three-Phase PLL Design

In grid-connected systems, a critical component of the converter's control system is the PLL, that provides phase angle and frequency measurements of the grid voltage for

control and protection purposes. Because the three-phase balanced source is used in the utility grid, a three-phase PLL is required.

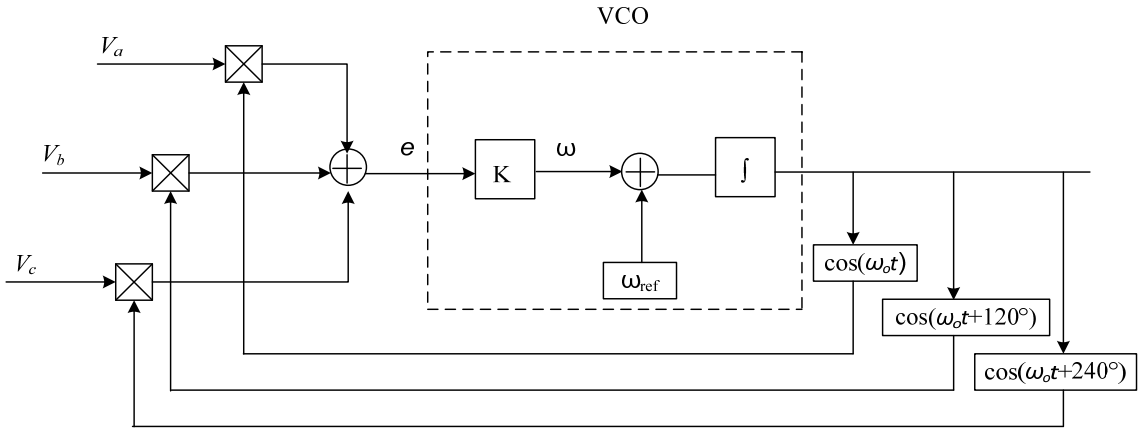

Fig. 22. Phase Locked Loop.

The input to the PLL, the three phase voltages V_a, V_b, V_c, is fed into multipliers that serve as phase detectors. Due to the balanced, three-phase sinusoidal signals in the grid, the three-phase voltages V_a, V_b, V_c are sinusoidal signals. To present the phase detection, three-phase voltages V_a, V_b, V_c should be multiplied by another sinusoidal signal that is phase shifted by 90° with respective to the three phase voltages [26]. This phase detection is represented mathematically as follows:

$$S_3(t) = S_1(t)S_2(t) \tag{4.1}$$

$$S_1(t) = A_1 \sin(\omega t + \theta_1(t)) \tag{4.2}$$

$$S_2(t) = A_2 \cos(\omega t + \theta_2(t)) \tag{4.3}$$

where S_1 is one of three phase sinusoidal signals, S_2 is the sinusoidal signal shifted by 90°, and S_3 is the product of S_1 and S_2.

The output of the multiplier is

$$S_3(t) = A_1 A_2 \sin(\omega t + \theta_1(t))\cos(\omega t + \theta_2(t))$$

$$= \frac{1}{2} A_1 A_2 \sin(\theta_1(t) - \theta_2(t)) + \frac{1}{2} A_1 A_2 \sin(2\omega t + \theta_1(t) + \theta_2(t)) \quad (4.4)$$

S_3(t) has two parts. The first one is a function of the phase difference only, while the second one is twice the signal frequency plus the two phases. As a result, the output of the multiplier consists of a DC signal, since the phase difference is independent on the function of frequency, and the signal at twice the fundamental frequency. The first term is called the error signal $S_e(t)$, that is,

$$S_e(t) = 0.5 A_1 A_2 \sin(\theta_1(t) - \theta_2(t)) \quad (4.5)$$

The error signal is zero when the phase difference is zero, which represents the phase locked state of a PLL. Any state results in a non-zero error signal except for the locked state. For the second term, the high frequency component needs to be removed. If it is a single-phase PLL system, a low-pass filter is used to remove the second harmonic term since it is not useful information [26].

An advantage of a three-phase PLL is to eliminate the need for the filter, as shown by (4.6). Due to the balanced three-phase source used in the grid, the phase of each input signal is shifted by 120°. Let $2\omega t + \theta_1(t) + \theta_2(t) = \varphi$, if the three input signals are added, then

$$0.5 A_1 A_2 \sin(\varphi) + 0.5 A_1 A_2 \sin(\varphi + 120^\circ) + 0.5 A_1 A_2 \sin(\varphi + 240^\circ) \quad (4.6)$$

$$= 0.5 A_1 A_2 (\sin(\varphi) + \sin(\varphi)(-\frac{1}{2}) + \cos(\varphi)(\frac{\sqrt{3}}{2}) + \sin(\varphi)(-\frac{1}{2}) + \cos(\varphi)(-\frac{\sqrt{3}}{2}))$$

$$= 0$$

Thus, under ideal conditions there is theoretically no second harmonic component presented. This reduces the filtering effort required for implementation. Thus, the total error signal for three phase results in a DC error signal

$$S_{err}(t) = \frac{3}{2} A_1 A_2 \sin(\theta_1(t) - \theta_2(t)) \tag{4.7}$$

To achieve a zero error signal, the voltage-controlled oscillator (VCO) described in Fig. 22 is used to change the phase of the feedback signals to match the phase of the input voltages V_a, V_b, V_c. A VCO is an electronic oscillator whose oscillation frequency is controlled by a voltage input. If the error signal is zero, then the VCO produces the desired frequency (60HZ), however, if the error signal is not zero, then the frequency is changed. Typically, the VCO has a constant K representing a change in the instantaneous frequency of the VCO as a function of the error signal (S_{err}),

$$K = \frac{d\omega}{de} \tag{4.8}$$

The feedback output signal of the VCO for each phase is given by

$$S_2(t) = A_2 \cos(\omega_{ref} t + \theta_2(t)) \tag{4.9}$$

The VCO produces a change in the output signal frequency as the error signal changes with time. The output frequency (ω_o) is written by the following relationship,

$$\omega_o = \omega_{ref} + Ke(t) \tag{4.10}$$

where ω_{ref} is the usual operating frequency (60Hz). Then by taking the integral of the output frequency ω_o to get the following relationship,

$$\omega_o t = \omega_{ref} t + K\int_0^t e(t)dt \tag{4.11}$$

$$\theta_2(t) = K\int_0^t e(t)dt \tag{4.12}$$

Thus as long as the error signal has a non-zero value, the output of the VCO signal will keep increasing until it equals $\theta_1(t)$. Substituting equation (4.12) into (4.7), $S_{err}(t)$ can be representes as

$$S_{err}(t) = \frac{3}{2} A_1 A_2 \sin(\theta_1(t) - K\int_0^t e(t)dt) \tag{4.13}$$

CHAPTER SIX

Simulation Results

This chapter discusses the simulation and testing of the PCS. First, the DC bus voltage is checked whether it is regulated by DC/DC converter to achieve a stable voltage. Second, the real and reactive output power of the inverter is verified whether they follow the fixed and dynamic load demand. Third, when the fuel cell power plant as a generator is connected to the grid, the real and reactive output power of the inverter is tested to keep the demand change well.

The PCS developed in this thesis was programmed in Matlab version 2009a. The fuel cell power plant mathematical model developed by Lukas, Lee and Ghezel-Ayagh [6-7] and the PCS was simulated in Matlab Simulink. The PCS built in Matlab Simulink can be found in the Appendix. Fig. 23 shows the flow diagram of the basic operation of the PCS between the fuel cell stack and the grid. The output power of the fuel cell stack is DC power, so it should be converted into AC power before transmit to the grid. By using the PCS, the wide range of the fuel cell stack output voltage is regulated to the desired voltage, V_{ref} ; and the power flow from the fuel cell stack to grid can be controlled based on the active and reactive reference power, P_{ref} and Q_{ref}.

6. 1 DC Bus Voltage

The output voltage of the fuel cell stack has a wide range; so the main task of the converter is to regulate the fuel cell stack voltage into a desired voltage, which is 480V. The stability of DC bus voltage needs to be checked first. The output voltage of DC/DC

converter model is shown in Fig. 24. The parameters for DC/DC converter and PI controller were given in Table 1 in Chapter Two.

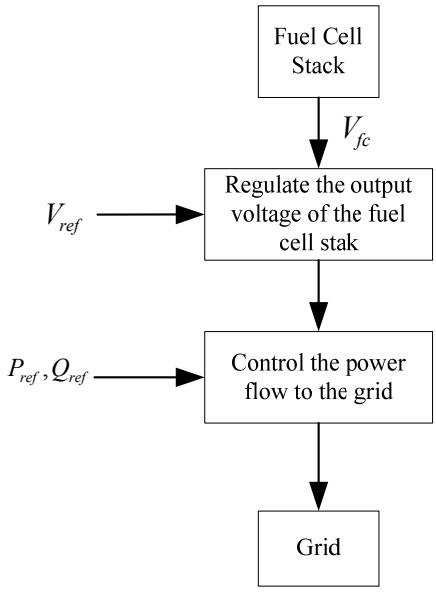

Fig. 23. Flow diagram of the basic operation of the PCS.

The voltage of fuel cell stack has been significantly regulated and stabilized only in 2 seconds as compared to the DFC/T output voltages shown in Fig. 5 in Chapter Two. The voltage in Fig. 5 is the results of 42 days of simulation data. Since the process is too slow and it is not necessary to run for 42 days of simulation data, and only 10 seconds of simulation results are shown here. In this first 10 seconds, the output voltage of hybrid DFC/T power plant varied significantly. However, as shown in Fig. 24, the output voltage of the DC/DC converter has regulated the voltage into a stable 480V in less than 2 seconds. Therefore, 10 seconds of simulation data is sufficient to prove its stability.

6. 2 Real and Reactive Power Flow Control

When the fuel cell power plant is connected to the grid, the real and reactive output power of the inverter should be controlled based on the load demand changes. It can be regulated by the inverter, and with the reference power demands, the output power of fuel cell should follow the power demands. The load demand can be a fixed load or a dynamic load. Generally, the reactive power is set to 10% of real power. Figs. 25 and 26 show the simulation with a fixed load in second units. The PCS follows the reference well in short time.

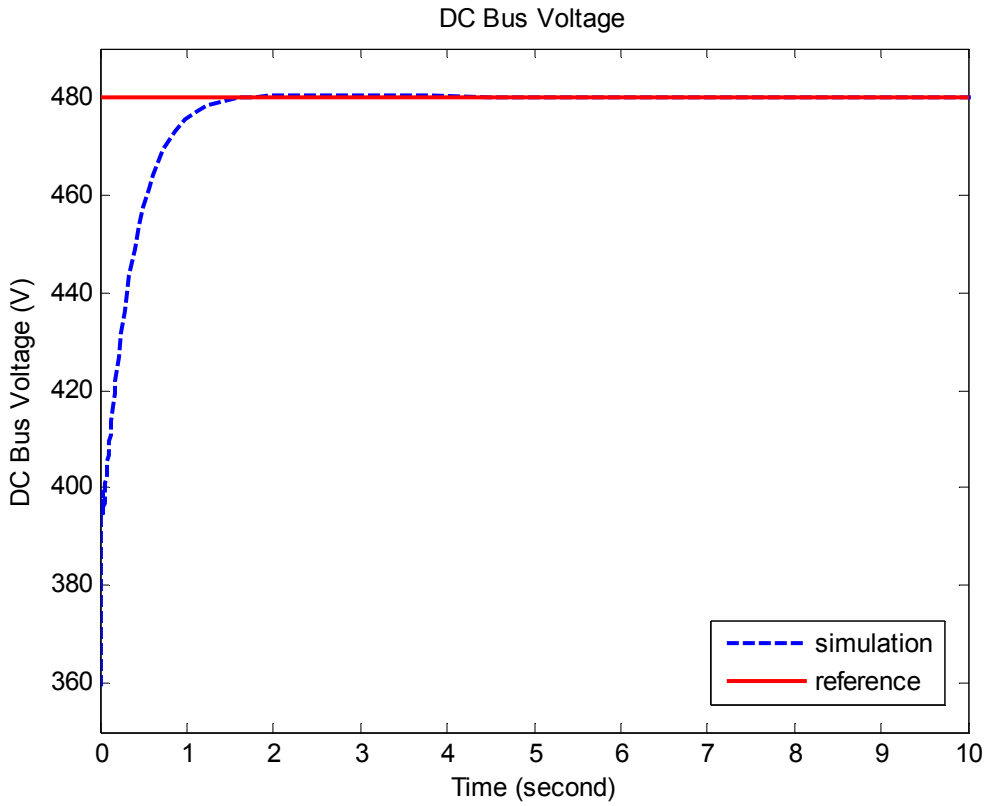

Fig. 24. DC bus Voltage.

The solid lines are the reference power point and the dot-dash lines are the actual power output. The result shows that active and reactive power are controlled to follow the power references set as P=100kW and Q=10kVar.

The averaged model of inverter follows the reference well in short time as shown in Figs. 25 and 26. The main task of the averaged model of inverter is to adapt the long-time simulation. Thus the result for long-time simulation should be checked. Figs. 27 and 28 show the long-time dynamic simulation for fuel cell. As known in the figures, the model follows the reference very closely in the long time period. The dashed lines are the reference power and the solid lines are the actual power output. When long-time simulation carry out, due to fuel-cell power plant connected with grid, we can set the frequency fixed in 60HZ.

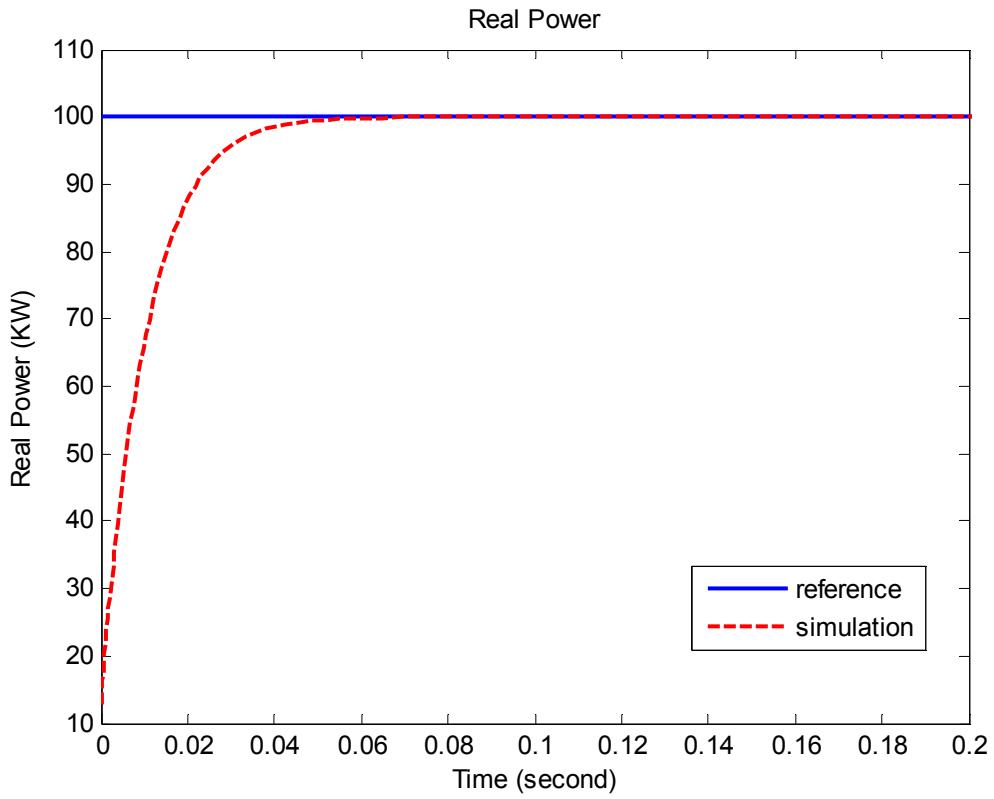

Fig. 25. Short-time simulation for real power.

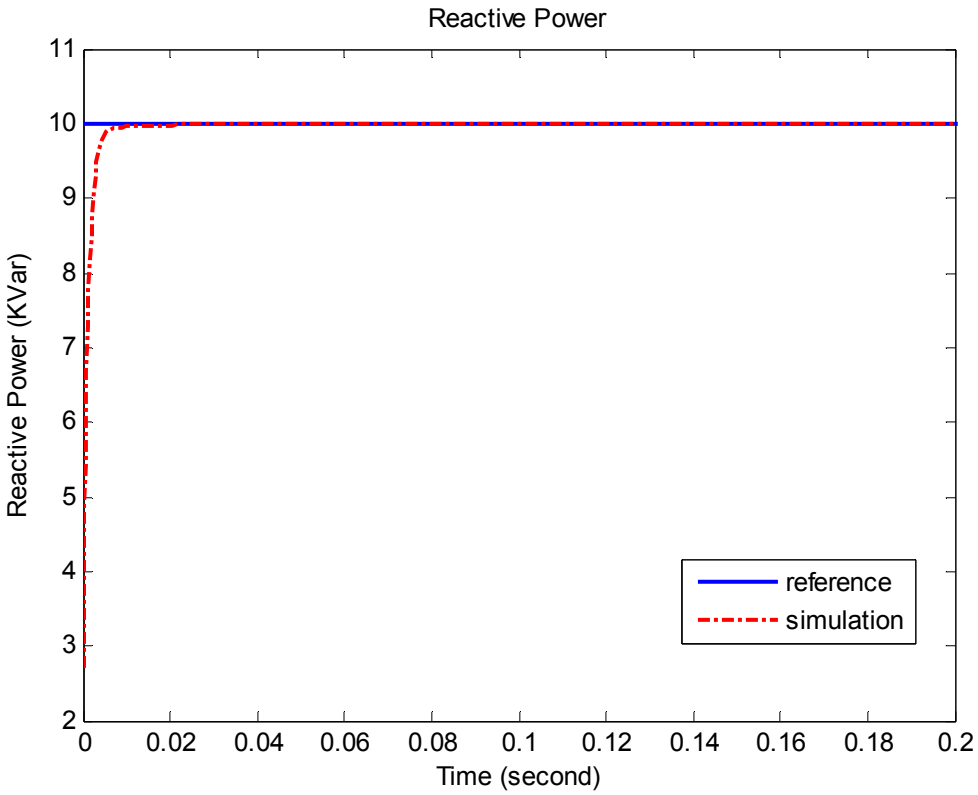

Fig. 26. Short-time simulation for reactive power.

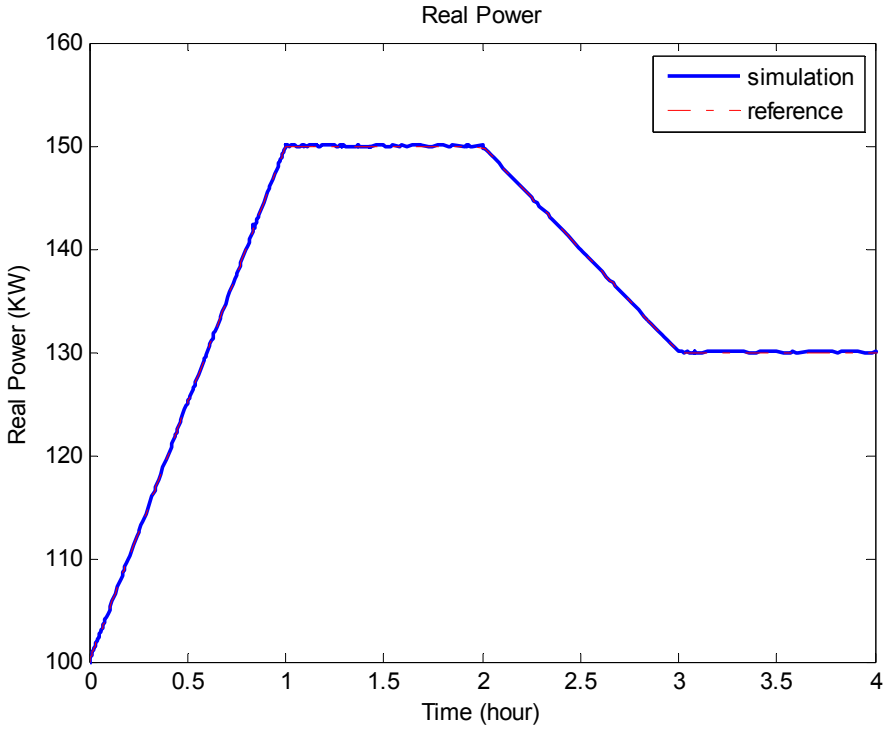

Fig. 27. Long-time simulation for real power.

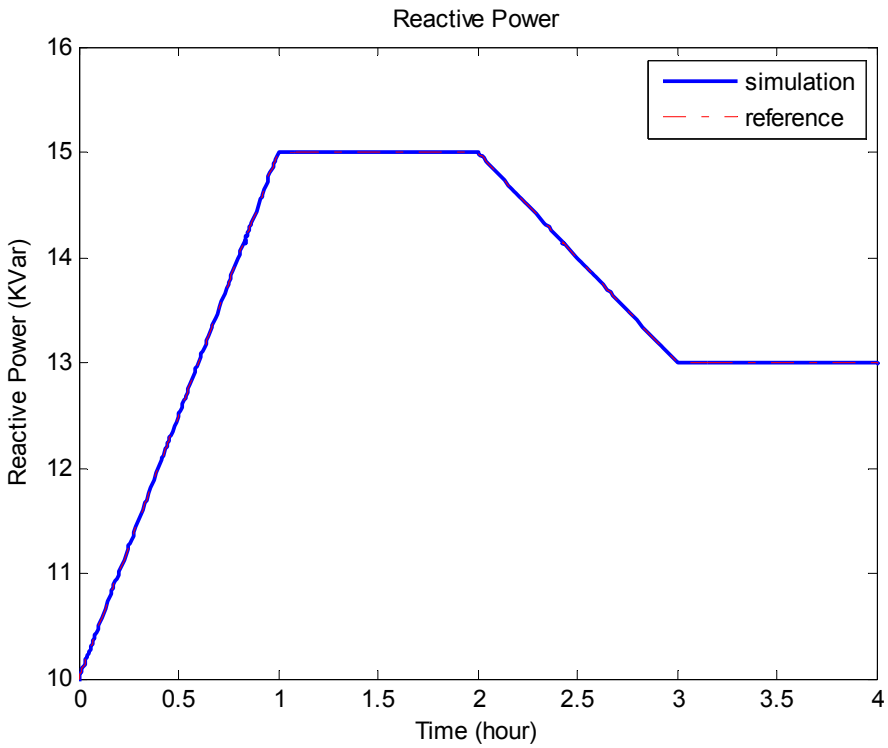

Fig. 28. Long-time simulation for reactive power.

As discussed in Chapter Four, real and reactive powers should be checked whether they follow load demand well when the fuel-cell power plant is considered as a generator in the power system. Fig. 29 shows the real and reactive power of the load demand. Real power is set to 120kW at the beginning of simulation, then it is increased to 160kW in 3600 seconds (one hour later), and finally it is dropped down to 140kW in 7200 seconds (two hours later). Reactive power is 10% of the real power and the set points are the same as the real power.

The four variables (P, Q, V, and δ) of the PV bus are needed to be calculated as the power reference for the fuel cell power plant. As shown in Fig. 20, because the bus connected to the fuel cell power plant is considered as the PV bus, the voltage magnitude and the real power are specified. Therefore, the rest of two variables, reactive power and

the voltage phase angle (Q, and δ), are determined. The calculation of the power flow is calculated by Newton-Raphson Method [36].

Figs. 30 and 31 show the four variables (P, Q, V, and δ) of the PV bus which is connected with the fuel cell power plant. Real power is fixed to 100kW, and reactive power varies depending on the load demand. The voltage magnitude is fixed to 1.03p.u. , and the voltage angle of the bus varies as well based on the load demand. Thus, the difference with simulation in Figs. 27 and 28 is that the voltage of grid-side changes with load demand. As shown in Fig. 32, the output reference of real power is 100kW. There are two small spikes in the figure because the voltage angle changes with dynamic demand and the same as in Fig. 33. Even though there are some small spikes in Figs. 32 and 33, the difference between the reference and simulation is within 1-2% so the performance is closed enough to the reference.

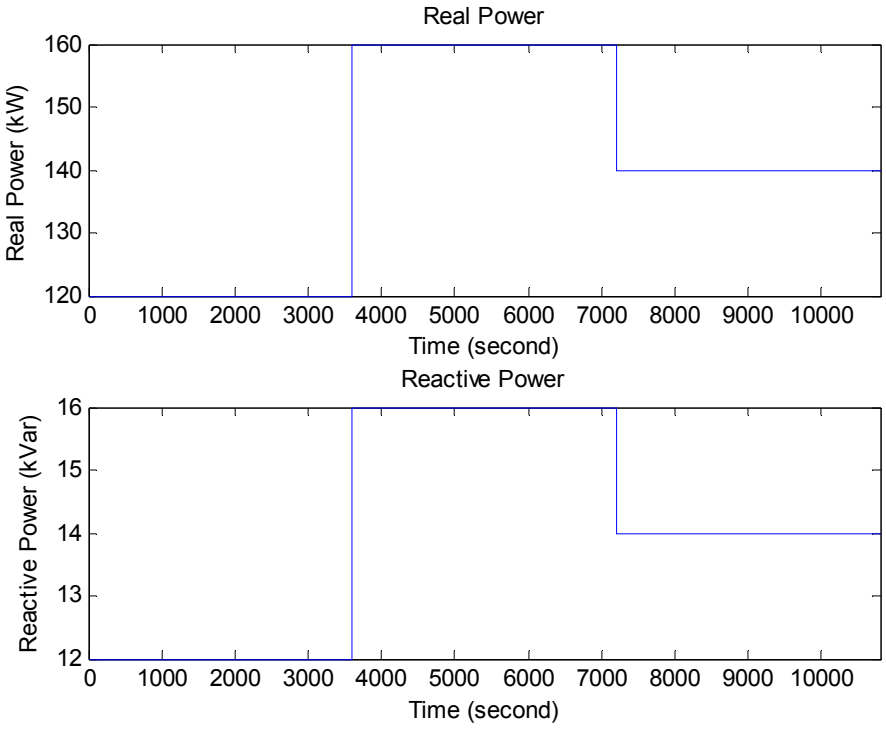

Fig. 29. Real and Reactive Power of Load Demand.

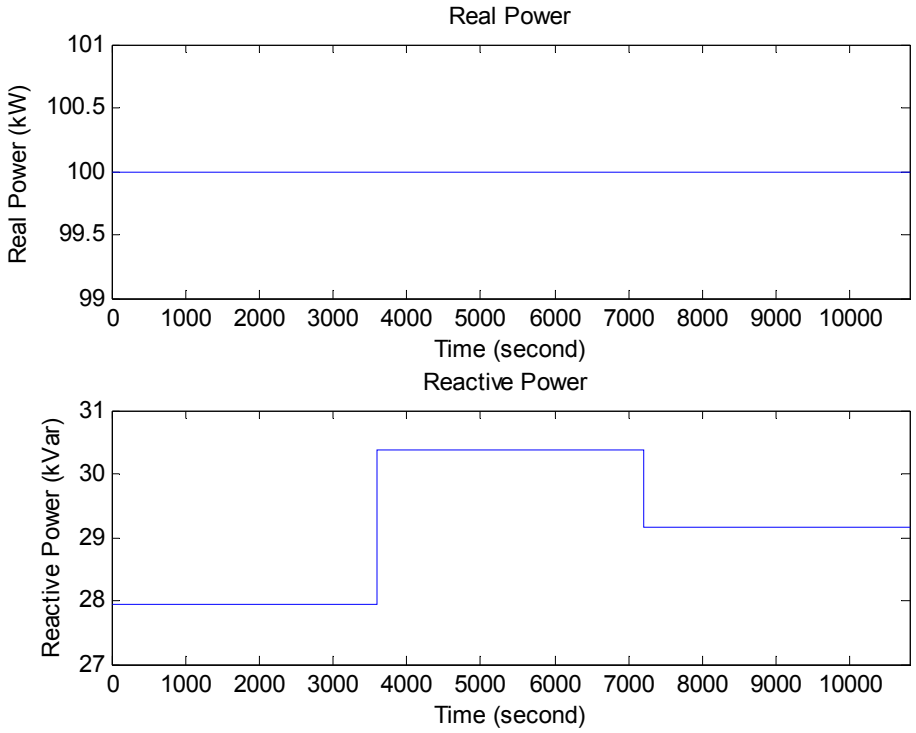

Fig. 30. Real and Reactive Power of PV Bus.

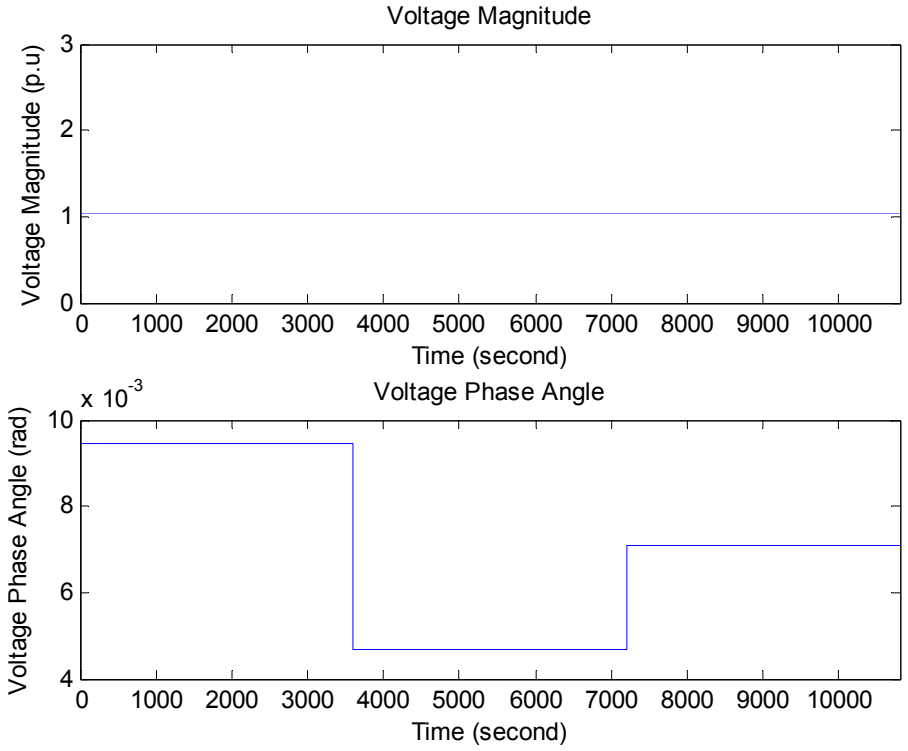

Fig. 31. The Voltage Magnitude and Phase Angle of PV bus.

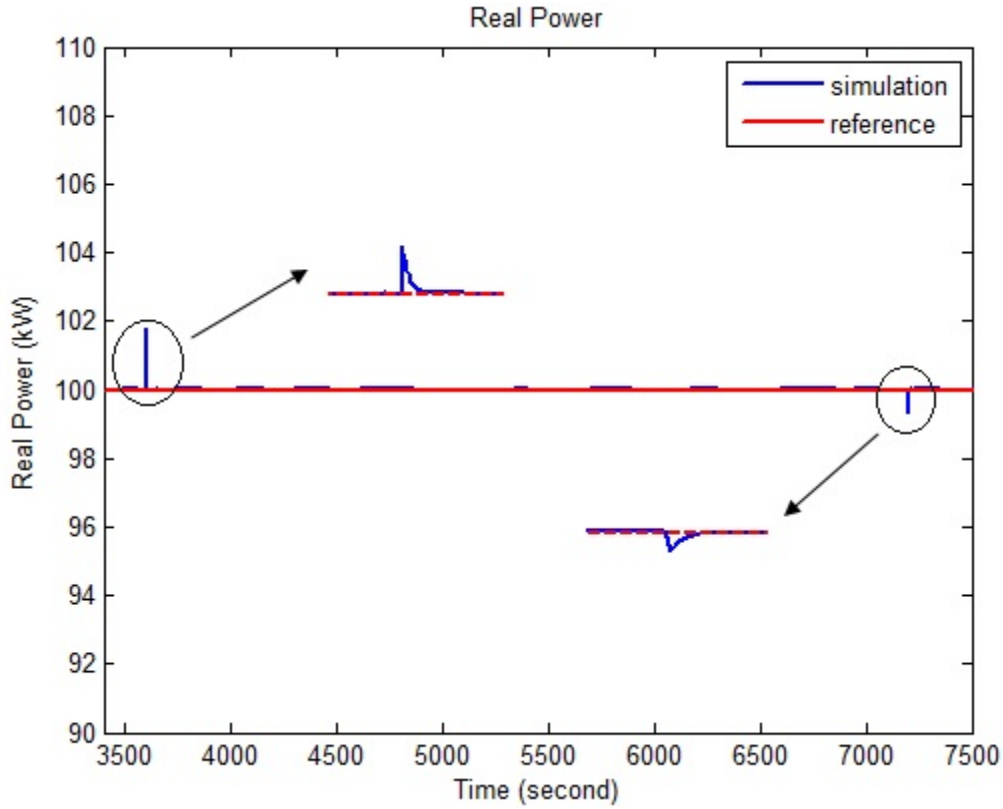

Fig. 32. Simulation of real power for fuel cell considered as a generator.

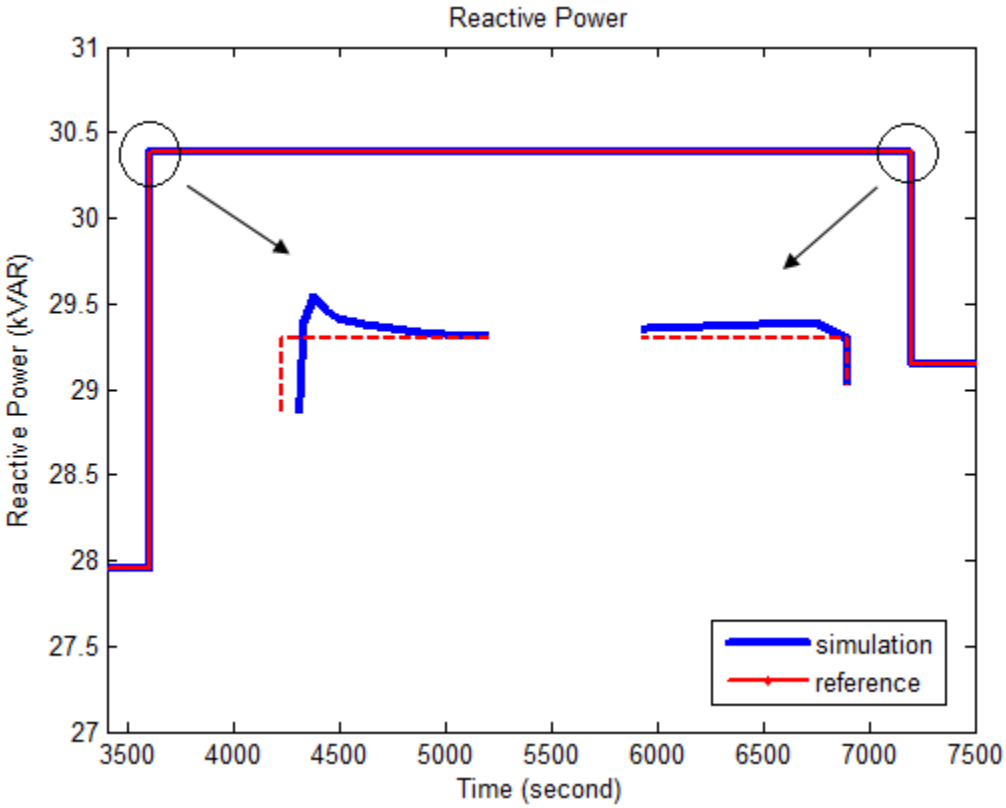

Fig. 33. Simulation of reactive power for fuel cell considered as a generator.

6. 3 Comparison with Detailed Model

In order to check the accuracy of the averaged model in the steady state, it is reasonable to compare the output power with the detailed model. Due to the high switching frequency in the detailed model, it is not practiced to run for a long time simulation, thus the test checks the result during a short time. The reference real and reactive powers give 160kW and 16kVar, respectively as shown in Figs 34 and 35. The solid line represents the output of detailed model and the dash-dot line is achieved from the averaged model. As one can observe from the figure, the averaged model is working very closely to the detailed model, and it is more accurate than the detailed one when following the reference.

The table 4 contains the elapsed time for the detailed model and the averaged model of the PCS. As shown in Table 4, the elapsed time of the averaged model is smaller than the detailed model; even the simulation speed is approximately increased by 7 times. Therefore, the averaged model is suitable to run the long time simulation.

Table 4:The Comparison of the Elapsed Time between the Detailed and Averaged Model.

Model	Elapsed Time for 3 seconds
The Detailed Model	132.8 seconds
The Averaged Model	21.6 seconds

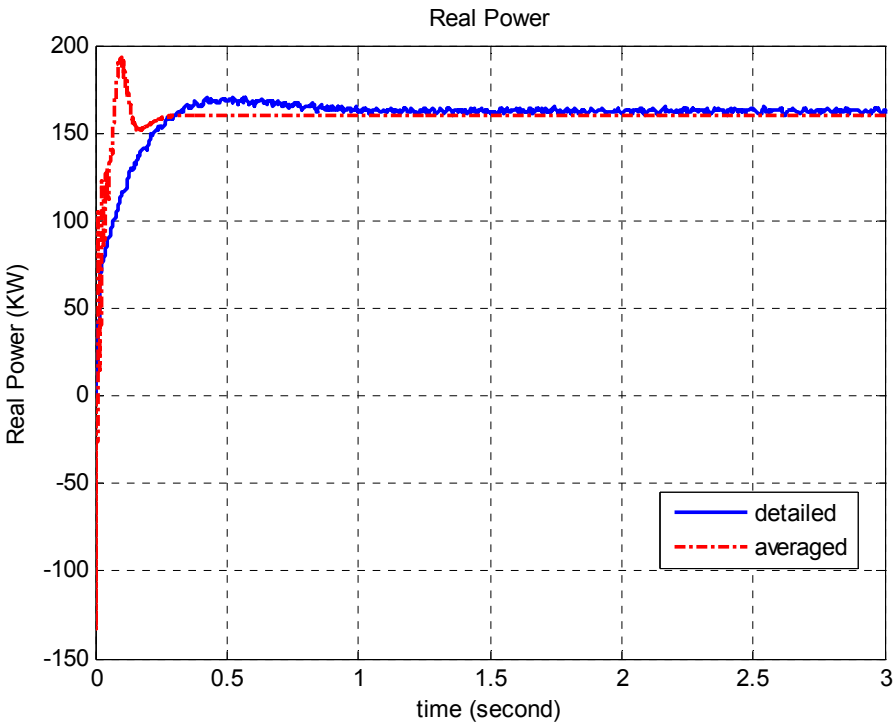

Fig. 34. Comparison of the real power output of two models.

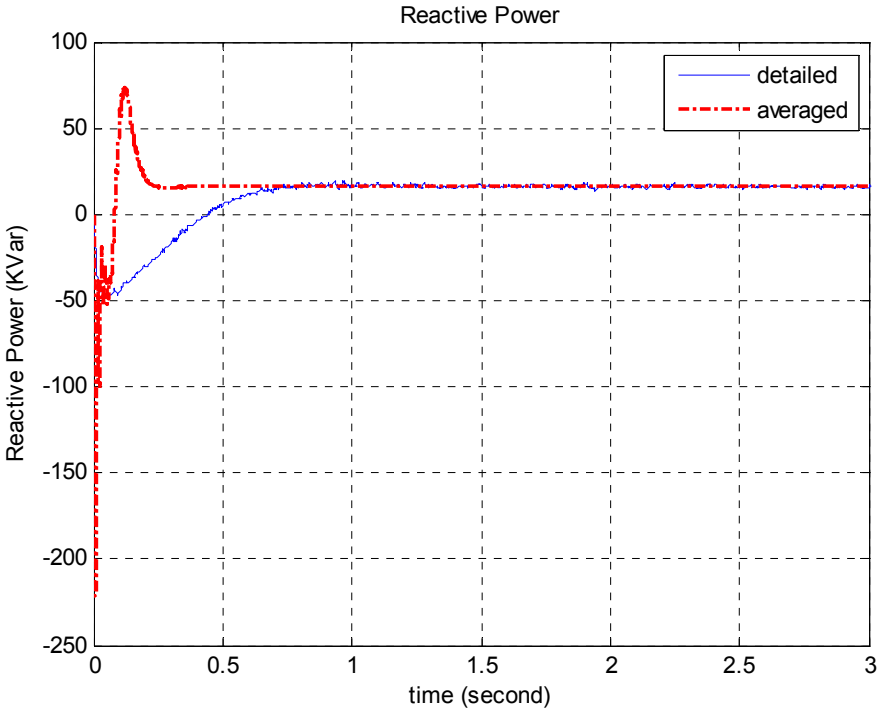

Fig. 35. Comparison of the reactive power output of two models.

CHAPTER SEVEN

Conclusion and Future Work

7.1 Conclusions

This thesis demonstrated the design and modeling of averaged methods of a power conditioning system (PCS) for the fuel cell power plant. There are two main tasks for the proposed PCS, which are DC link voltage regulation and power flow control. The main purpose of using the averaged model of PCS instead of detailed model is for a long-time simulation such as several hours or days. It is also suitable to run the simulation for the fuel cell power plant connected to the grid.

For control strategies of each subsystem, the PI controller is adopted in the Buck-Boost DC/DC converter and inverter control system, and stability for each control system is analyzed.

The simulation results have validated the proposed PCS system. The results showed the proposed PCS can control the power flow very well to follow the active and reactive power reference for both short- and long-time simulation.

7.2 Future Work

The proposed averaged models of PCS improve the calculation speed, so it is suitable for studying the transient stability of fuel-cell power plant in grid-connected and standalone mode. When the fuel-cell power plant is in standalone mode, voltage and frequency droop control can be adapted to control the micro-grid. Due to disconnection from the grid, variations of frequency should be regulated. Thus, additional studies and

developments are needed to maintain the stability in the transient mode and standalone mode.

APPENDIX

APPENDIX

The PCS in Matlab Simulink

The Fig. 36 shows the PCS built in Matlab Simulink. There are five main parts: DC/DC converter, DC/AC inverter, the feedback control for the DC bus voltage, the PQ controller for the inverter and the interface to calculate the data in PV bus.

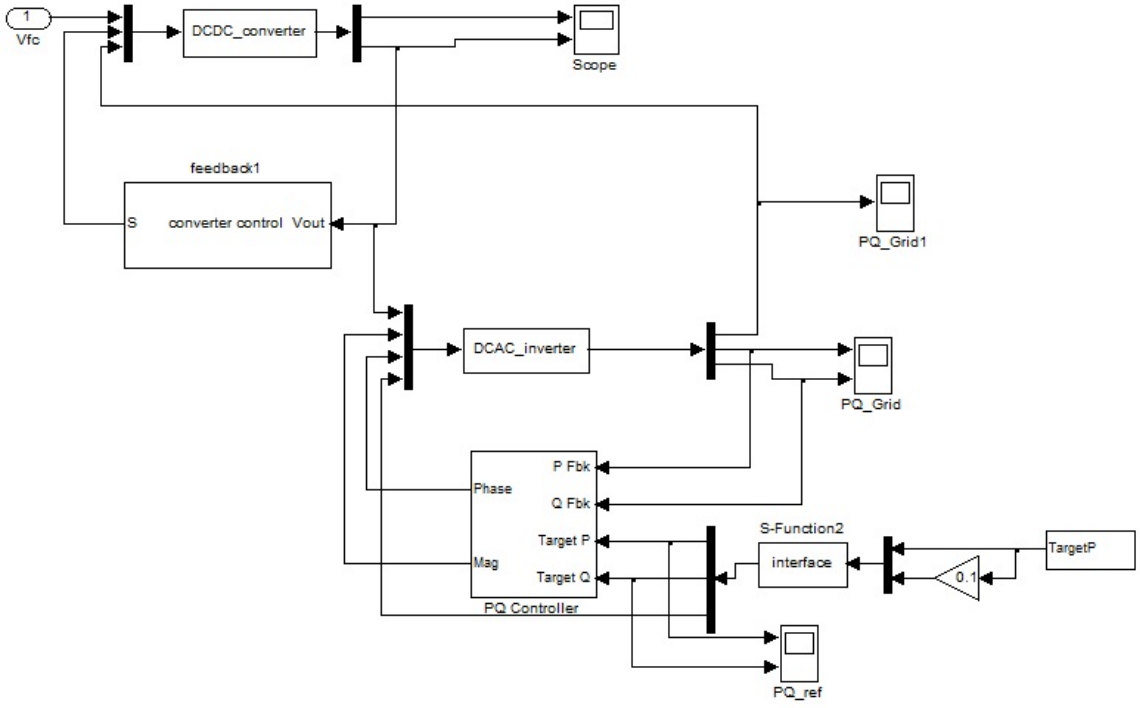

Fig. 36. The PCS in Matlab Simulink.

BIBLIOGRAPHY

[1] DOE; The Potential Benefits of Distributed Generation and Rate-Related Issues that May Impede Their Expansion; 2007.

[2] A. M. Shipley and R. N. Elliott, "Stationary fuel cells: future promise, current hype," American Council for an Energy-Efficient Economy, March, 2004.

[3] W. Yang, "An intelligent control system for a hybrid fuel cell with gas turbine power plant," Ph.D. Dissertation, The Pennsylvania State University, University Park, PA, USA, 2009.

[4] "Fuel cell handbook," EG&G Technical Services, Inc., November, 2004.

[5] U.S. Department of Energy, "Fuel Cell Technologies Program"<URL: http://www1.eere.energy.gov/hydrogenandfuelcells/fuelcells/pdfs/fc_comparison_chart.pdf>

[6] M. D. Lukas, K. Y. Lee, and H. Ghezel-ayagh, "An explicit dynamic model for direct reforming carbonate fuel cell stack," *IEEE Trans. Energy Conversion*, vol. 16, pp. 289-295, September, 2001.

[7] M. D. Lukas, K. Y. Lee, and H. Ghezel-ayagh, "Modeling and cycling control of carbonate fuel cell power plants," *Control Engineering Practice*, vol. 10, pp. 197-206, April, 2001.

[8] W. Yang, K. Y. Lee, T. Junker, and H. Ghezel-ayagh, "Model augmentation for hybrid fuel-cell/gas tur*bine power plant," in Proc. of the IEEE Power Energy Society General Meeting*, Pittsburth, PA, July 26-30, 2009, pp.1-8.

[9] W. Yang, K. Y. Lee, T. Junker, and H. Ghezel-ayagh, "Fuzzy fault diagnosis and accommodation system for hybrid fuel-gas/gas-turbine power plant," *IEEE Trans. on Energy Conversion*, Vol. 25, No. 4, pp.1187-1194, December, 2010.

[10] W. Yang and K. Y. Lee, "An optimal reference governor with a neural network combined model for hybrid fuel-cell/gas turbine," *IEEE Power Energy Society General Meeting*, Minneapolis, MN, July 25-29, 2010, pp.1-6.

[11] T. Choi and K. Y. Lee, "Intelligent control of a fuel cell power plant," in *Proc. of the 17th IFAC World Congress*, Seoul, Korea, July 6-11, 2008, pp. 15915–15920.

[12] J. S. Lai, "Power conditioning circuit topologies," *IEEE Industry Electronics Magazine*, June, 2009, pp. 24-34.

[13] T. Choi and K. Y. Lee, "Interface of a fuel cell distributed generator with distribution system network," *in Proc. of the IEEE Power Energy Society General Meeting*, Calgary, Canada, July 26-30, 2009.

[14] N. Mohan, T. Undeland, and W. Robbins, *Power Electronics: Converters, Applications, and Design*, Wiley: New York, USA, 2002.

[15] C. Wang, M. H. Nehrir, and H. Gao, "Control of PEM fuel cell distributed generation system," *IEEE Trans. On Energy Conversion*, Vol. 21, No.2, pp.586-595, June, 2006.

[16] T. Bjazic, Z. Ban, and I. Volaric, "Control of a fuel cell stack loaded with DC/DC boost converter," *IEEE International Symposium on Industry Electronics*, Cambridge, UK, June30-July2, 2008, pp. 1489-1494.

[17] R. Wang, J. Liu, Y. Chen, and Z. Wang, "A state-space model for steady-state analysis of soft-switching PWM DC/DC converters based on MATLAB/Simulink," *The 4th International conference on Power Electronics and Motion Control*, Xi'an, China, August 14-16, 2004, pp. 1706-1710.

[18] S. E. Beid, S. Doubabi, and M. Chaoui, "Adaptive control of PWM DC-to-DC converters operating in continuous conduction mode," *IEEE Mediterranean Conference on Control and Automation*, Athens, Greece, July 27-29, 2007, pp. 1-5.

[19] R. Dorf and R. Bishop, *Modern Control Systems*, Prentice Hall: Upper Saddle River, USA, 2010.

[20] Z. Ye, R. Walling, L. Grarces, R. Zhou, L.Li, and T. Wang, "Study and Development of Anti-islanding Control for Grid-Connected Inverters," General Electric Global Research Center, Niskayuna, New York, May 2004.

[21] E. Figueres, G. Garcerá, J. Sandia, F. González-Espín, and J. Calvo Rubio "Sensitivity Study of the Dynamics of Threee-Phase Photovoltaic Inverters With an LCL Grid Filter," *IEEE Trans. on Industrial Electronics*, Vol. 56, No. 3, pp. 706-717, March, 2009.

[22] F. Z. Peng, Y. W. Li and L. M. Tolbert, "Control and Protection of Power Electronics Interfaced Distributed Generation Systems in a Customer-Driven Microgrid," *IEEE Conference on Power & Energy Society General Meeting*, 2009.

[23] M. Dai, "Control of power converters for distributed generation applications," PhD dissertation, The Ohio State University, Columbus, OH, USA, 2005.

[24] J. D. Glover, M. S. Sarma, and T. J. Overbye, *Power System Analysis and Design*, Thomson: Toronto, Canada, 2008.

[25] H. Awad, J. Svensson, and M. J. Bollen, "Tuning Software Phase-Locked Loop for Series-Connected Converters", *IEEE Transactions on Power Delivery*, Vol. 20, No. 1, pp. 300-308, Jan. 2005.

[26] W. Phipps, M. J. Harrison, and R. M. Duke, "Three-Phase Phase-Locked Loop Control of a New Generation Power Converter," *1st IEEE Conference on Industrial Electronics and Applications*, 2006.

[27] L.N. Arruda, S.M. Silva, and B.J.C. Filho, "PLL Structures for Utility Connected Systems," *IEEE/IAS'01*, pp. 2655-2660, 2001.

[28] M. Dai, M. N. Marwali, J. Woo, and A. Keyhani, "Power control of a single distributed generation unit," *IEEE Trans. on Power Electronics*, Vol. 23, No. 1, pp. 343-352, January, 2008.

[29] C. Wang, "Modeling and control of hybrid wind/photovoltaic/fuel cell distributed generation systems," PhD Dissertation, The Montana State University, Bozeman, MT, USA, 2006.

[30] C. Wang, M. H. Nehrir, and H. Gao, "Control of PEM fuel cell distributed generation systems," *IEEE Trans. on Energy Conversion*, Vol. 21, No. 2, pp. 586-595, June, 2006.

[31] P. Kundur, *Power System Stability and Control*, McGraw-Hill: California, USA, 1994.

[32] X. Wang and L. Zhao, "Simulation of charge-discharge control strategy of bi-directional inverter in grid-connected mode," *International Conference on Intelligent Technology and Automation*, May11-12, Changsha, China, vol. 3, pp. 322-325.

[33] S. K. Mazumder, R. K. Burra, R. Huang, M. Tahir, and K. Acharya, "A Univeral Grid-connected Fuel-Cell Inverter for Residential Application," *IEEE Trans. on Industrial Electronics*, Vol. 57, No. 10, October, 2010.

[34] B. S. Prasad, S. Jain, and V. Agarwal, "Universal single-stage grid-connected inverter," *IEEE Trans. Energy Convers.*, Vol. 23, No. 1, pp. 128-137, Mar. 2008.

[35] Q. Chongming and K. M. Smedley, "Three-phase grid-connected inverters interface for alternative energy sources with unified constant-frequency integration control," in *Conf. Rec. IEEE IAS Annu. Meeting*, 2001.

[36] H. Saadat, *Power System Analysis*, McGraw-Hill: New York, USA, 1999.